UNIVERSIDADE
BEIRA INTERIOR

Development of Multifunctional Hydrogel for Cancer Therapy

Ivo João Viana Sabino

Dissertação para obtenção do Grau de Mestre em
Ciências Biomédicas
(2º Ciclo de Estudos)

Orientador: Prof. Doutor Ilídio Joaquim Sobreira Correia
Co-orientador: Doutor Duarte Miguel de Melo Diogo
Co-orientador: Mestre Cátia Gomes Alves

outubro de 2020

"The only place success comes before work is in the dictionary."

Vince Lombardi

Por e para ti, Pai…
(Não era suposto ser assim. Mas não o consigo fazer de outra maneira.)

Agradecimentos

Desde a minha entrada no laboratório até à entrega desta Dissertação de Mestrado passaram-se, aproximadamente, 500 dias onde muita, mas mesmo muita coisa aconteceu. Este ano que passou teve de tudo um pouco: imprevisibilidade, (muito) trabalho, desgaste e muito sofrimento. Ainda assim, culminou, entre outras conquistas, nesta Dissertação. E, para tal, existiram diversas pessoas que foram fundamentais e às quais quero e tenho o dever de agradecer.

Em primeira instância, o meu agradecimento ao Professor Doutor Ilídio Correia por ter aceite ser meu orientador na obtenção do meu Grau de Mestre em Ciências Biomédicas. Como sempre me foi dito, o progresso académico são como que portas que se vão abrindo na construção do nosso futuro. E, felizmente, tive a possibilidade de abrir mais uma dessas portas. Para além disso, o meu obrigado pela exigência e rigor pela qual sempre pautou todas as suas intervenções, e também por me ter providenciando os meios materiais necessários à realização de um trabalho científico de qualidade. Gostaria ainda de agradecer toda a confiança que sempre demonstrou em mim, nos mais diversos assuntos. Por fim, gostaria ainda de referir que lhe estou grato pela presença e apoio naquela terça-feira, dia vinte e oito de janeiro de dois mil e vinte.

Ao meu co-orientador, Doutor Duarte Diogo, gostaria de dizer obrigado. Obrigado por todo o auxílio. Na escrita do meu artigo de revisão e na execução desta Dissertação. Obrigado pelas dicas. Obrigado pelo sem-número de ensinamentos e correções. Obrigado por me ajudar a encontrar sempre uma alternativa, quando os problemas surgiam. E obrigado (como não poderia deixar de ser) pelas mensagens de apoio e cuidado que me endereçou durante aquele mês negro e de muito sofrimento. Sei que, apesar de fisicamente ausente, esteve comigo em pensamento. Obrigado!

Às Mestres Cátia Alves (minha co-orientadora) e Ana Rita Sousa (minha "pseudo-co-orientadora"). Se no início do meu ano de Dissertação estava receoso pela súbita troca de coorientadores e, consequentemente, do meu plano de trabalhos, esse medo rapidamente esfumou-se pois as duas deixaram-me calmo, e demonstraram uma enorme e pronta disponibilidade para me ajudar. E para me transmitirem todos os ensinamentos teórico-práticos que apreenderam das mais diversas formas, ao longo destes anos – acreditem que foram, muitas vezes, como que um 'tradutor'. Obrigado pela (muita) paciência com as minhas 1001 dúvidas e questões. Obrigado pela compreensão para com os meus erros. Deixem-me ainda dizer-vos que admiro o mútuo companheirismo e

entreajuda que têm as duas. Tenho a sorte de poder afirmar que não tive dois, mas sim três coorientadores! Por fim, não poderia não expressar a minha profunda gratidão por me terem acompanhado naquele que foi o dia mais negro dos meus vinte e dois (quase três) anos de vida. Significou muito para mim. Obrigado!

Ao Miguel e à Ariana. Sempre me disseram (e era algo que estranhava) que seria na faculdade que encontraria amigos que ficariam para toda uma vida. Mas vocês vieram provar que todas essas pessoas estavam corretas. Ao bom fundo que vos é caraterístico, há ainda a juntar a amizade que tiveram comigo e os muitos e bons momentos que passamos ao longo destes, já longos, cinco anos. Mesmo longe dos que me são queridos, a vossa amizade ajudou-me a ultrapassar as normais saudades de casa. Apesar de tudo o que passámos, estivemos juntos. Aprendemos e ajudámo-nos mutuamente. Nos momentos bons e nos menos bons. E foi nestes últimos que vi a sorte que tenho. Desde o levarem-me a casa, às mensagens, ao apoio que me foram dando ao longo daquela minha jornada de dor e sofrimento, a tudo. Agradeço terem entrado na minha vida. Oxalá a distância que nos possa separar seja apenas física. Estar-vos-ei eternamente grato.

Agradeço aos restantes elementos do grupo de investigação no qual estive inserido durante este ano. Votos de sucessos pessoais e profissionais.

De igual forma, devo um especial agradecimento a outras (outrora) pessoas, mas agora amigos do coração que a vida me foi presenteando, quer na Alenquer, quer em São Bernardino, quer na Covilhã. Cada um deles, à sua maneira, esteve comigo. Ligou-me, mandou-me uma mensagem, deu-me um abraço ou um "Força!" e, acima de tudo, foi acreditando em mim, quando a minha crença era quase nula. Fizeram-me não desistir, quando era esse o caminho mais fácil. Apoiaram-me, motivaram-me, animaram-me, preocuparam-se comigo. Apesar da distância, mostraram que estão ao meu lado. Não desde sempre. Mas, certamente, para sempre. A cada um deles – Mónica; Catarina C.; Ana Beatriz; Rodrigo; Helena; Ana Margarida; Joana; Manuela e Inês; Filipa, Catarina e Carolina; Ana Paula, André, Pedro e Maria; e Joel – o meu mais profundo e sincero, obrigado. Muito obrigado! Sou um enorme privilegiado por ter sido abençoado e presenteado com a vossa amizade.

Gostaria ainda de agradecer, de um modo especial, à Doutora Elisabete Costa. Apesar de longe, nunca me negou um conselho, um esclarecimento, uma ajuda nas dúvidas e questões que me foram surgindo, aquando da pesquisa bibliográfica sobre as mais diversas temáticas presentes no meu artigo de revisão. Quero igualmente agradecer o apoio que me deu, mal soube do infortúnio pelo qual eu e a minha família passámos.

Obrigado por fazer jus à expressão: “Estou aqui, à distância de uma mensagem/chamada”.

Por fim mas, sem dúvida, não menos importante, um enorme obrigado à minha Família. Confesso que não sei o que dizer. Estou sem palavras. É graças a cada um de vós que eu aqui estou. Ao vosso amor, ao vosso apoio, ao vosso empenho, aos vossos esforços. Devo-vos tudo o que tenho. Ajudaram-me a crescer e a tornar-me no ser humano que sou hoje. Estiveram comigo desde o princípio dos princípios. Nas vitórias, congratularam-me. E congratularam-se com elas, pois também foram vossas. Nas derrotas, ajudaram-me a aprender com elas e a reagir. Ampararam-me, orientaram-me e aconselharam-me. Nada neste mundo é mais forte que aquilo que nos une. Nada mesmo! O amor e alegria que sentimos nos nossos corações quando estamos juntos é um sentimento inexplicavelmente único e especial. Que me inspira todos os dias a fazer melhor. A ser melhor! Foram, são e sempre serão o meu sustento, o meu porto seguro. São o meu maior orgulho. E todo este parágrafo continua a ser a mais pura das verdades, mesmo após a tragédia que se abateu sobre nós no início deste ano. Porque a presença dele é inegável. Em tudo! Se, em certas dificuldades, não fui abaixo, certamente a ele o devo. Depois de tudo isto, senti em mim uma presença, que não tem uma explicação lógica ou racional. Espero que, esteja ele onde estiver, sinta orgulho em mim e nesta minha conquista, como eu me orgulho de lhe ter podido chamar ‘Pai’. És a minha maior referência e o meu maior exemplo. Que nos orientes nesta caminhada que é a Vida. Amo-vos! […]

E obrigado a Deus! Pela oportunidade que me está a dar de tentar ser feliz!

Resumo

O cancro da mama é uma das doenças com maior mortalidade em todo o mundo, que afeta sobretudo o sexo feminino. Este facto está relacionado com as limitações associadas às terapias aplicadas em meio clínico (quimioterapia e radioterapia), que apresentam uma baixa eficiência, toxicidade inespecífica, e ainda causam efeitos secundários nos pacientes. Deste modo, é essencial o desenvolvimento de estratégias terapêuticas inovadoras que apresentem uma maior eficácia e segurança.

Entre as diferentes abordagens terapêuticas atualmente a serem desenvolvidas, a terapia quimio-fototérmica mediada por nanomateriais tem apresentado resultados promissores. Esta modalidade terapêutica explora possíveis efeitos sinérgicos entre a aplicação localizada de hipertermia, mediada por nanomateriais responsivos à luz com um comprimento de onda na região do infravermelho próximo (em inglês: *Near Infrared* (NIR)) e que mediam a entrega direcionada de fármacos. No entanto, as nanopartículas administradas sistemicamente apresentam uma taxa de acumulação no tumor inferior a 1 %. Com o intuito de incrementar a acumulação dos nanomateriais no tumor, a entrega destes diretamente no local do tumor através de matrizes poliméricas tridimensionais injetáveis tem vindo a ser cada vez mais explorada.

Nesta Dissertação de Mestrado, foi desenvolvido um hidrogel de quitosano injetável que gelificava *in situ* através de reticulação ionotrópica. Para além disso, foram também incorporadas nanopartículas de Albumina de Soro Bovino contendo IR780 (agente fototérmico; IR/BPN) e nanopartículas de Succinato de D-α-Tocoferil Polietilenoglicol 1000 encapsulando Doxorubicina (fármaco quimioterapêutico; DOX/TPN) no hidrogel, de modo a explorar o potencial desta matriz na terapia quimio-fototérmica do cancro. Os resultados obtidos permitiram confirmar que os hidrogéis produzidos (IR/BPN@Gel e IR/BPN+DOX/TPN@Gel) apresentaram boas propriedades físico-químicas para aplicação na terapia do cancro. Quando irradiados com luz NIR, o IR/BPN@Gel e IR/BPN+DOX/TPN@Gel induziram um aumento de temperatura de 9.2 °C e 9.0 °C, respetivamente, confirmando o seu potencial fototérmico. Esta interação com a luz NIR também aumentou em 1.7 vezes a libertação de DOX do hidrogel.

Para além disso, nos estudos *in vitro* foi demonstrada a citocompatibilidade do IR/BPN@Gel. Este sistema não induziu qualquer efeito citotóxico em células normais ou em células cancerígenas. Para além disto, a irradiação do IR/BPN@Gel com a luz NIR (terapia fototérmica) causou uma redução (em 65 %) da viabilidade de células do cancro

da mama. O IR/BPN+DOX/TPN@Gel sem ser irradiado (quimioterapia) apenas reduziu a viabilidade celular em 15 %. Por outro lado, a terapia quimio-fototérmica mediada pelo IR/BPN+DOX/TPN@Gel reduziu a viabilidade das células em 91 %. Os resultados obtidos demonstram o potencial deste hidrogel injetável (com formação *in situ*) para aplicação na terapia quimio-fototérmica de células do cancro da mama.

Palavras-chave

Cancro;Doxorrubicina;Entrega Localizada;Hidrogel Injetável;IR780;Terapia Quimio-Fototérmica

Resumo Alargado

Atualmente, o cancro é uma das doenças com maior taxa de mortalidade associada. Particularmente, o cancro da mama, que afeta sobretudo o sexo feminino, é dos mais frequentes e letais. Tal facto, é explicado pelas limitações apresentadas pelas terapias usadas em meio clínico (quimioterapia e radioterapia) que, para além de apresentarem uma eficácia reduzida, induzem toxicidade sistémica, de que resultam efeitos secundários para os pacientes. Deste modo, torna-se imprescindível o desenvolvimento de novas estratégias terapêuticas que sejam mais eficazes e seguras.

De entre as diferentes abordagens terapêuticas atualmente a serem desenvolvidas, a terapia quimio-fototérmica mediada por nanomateriais tem apresentado resultados promissores na terapia do cancro. Esta abordagem terapêutica faz uso das propriedades físico-químicas das nanopartículas, que permitem que estas se acumulem na região tumoral. A zona do tumor, ao ser posteriormente irradiada com uma luz com um comprimento de onda na região do infravermelho próximo (750-1000 nm; do inglês: *Near Infrared* (NIR)), sofre um aumento de temperatura, devido à interação desta radiação com os nanomateriais. Este incremento de temperatura pode induzir a morte das células cancerígenas. A baixa interação desta radiação com os diferentes componentes biológicos (como a água, a melanina ou a hemoglobina) e a sua elevada capacidade de penetração nos tecidos enfatizam a importância da utilização da luz NIR no tratamento do cancro. Por outro lado, o aumento de temperatura pode levar à libertação do fármaco quimioterapêutico armazenado no nanomaterial, levando a um efeito sinérgico. Contudo, as nanopartículas administradas sistemicamente apresentam uma taxa de acumulação no tumor inferior a 1 %. Recentemente, a entrega direta de nanopartículas no tumor por matrizes poliméricas tridimensionais injetáveis tem demonstrado resultados promissores.

Durante o meu 2.º Ano de Mestrado, foi desenvolvido um hidrogel de quitosano injetável que gelificava *in situ* através de reticulação ionotrópica. Para além disso, procedi também à incorporação de nanopartículas de Albumina de Soro Bovino contendo IR780 (agente fototérmico; IR/BPN) e nanopartículas de Succinato de D-α-Tocoferil Polietilenoglicol 1000 encapsulando Doxorubicina (fármaco quimioterapêutico; DOX/TPN) no hidrogel. Esta abordagem tinha como objetivo explorar o potencial desta matriz na terapia quimio-fototérmica do cancro. Os resultados obtidos permitiram confirmar que os hidrogéis produzidos (IR/BPN@Gel e IR/BPN+DOX/TPN@Gel) apresentaram boas propriedades

físico-químicas para aplicação na terapia do cancro. Quando irradiados com luz NIR, o IR/BPN@Gel e IR/BPN+DOX/TPN@Gel induziram um aumento de temperatura de 9.2 °C e 9.0 °C, respetivamente, confirmando o seu potencial fototérmico. Esta interação com a luz NIR também aumentou em 1.7 vezes a libertação de DOX do hidrogel.

Por outro lado, nos estudos *in vitro* foi demonstrada a citocompatibilidade do IR/BPN@Gel. A irradiação do IR/BPN@Gel com a luz NIR (terapia fototérmica) causou uma redução (em 65 %) da viabilidade de células do cancro da mama. O IR/BPN+DOX/TPN@Gel sem ser irradiado (quimioterapia) apenas reduziu a viabilidade celular em 15 %, enquanto que a terapia quimio-fototérmica mediada pelo IR/BPN+DOX/TPN@Gel reduziu a viabilidade das células em cerca de 91 %. Os resultados obtidos demonstram o potencial deste hidrogel injetável (com formação *in situ*) para aplicação na terapia quimio-fototérmica do cancro da mama.

Abstract

Breast cancer continues to be one of the most frequently diagnosed cancers, having also one of the highest mortality rates among women. This scenario is justified by the limitations associated with the therapies currently used in the clinic (namely chemotherapy and radiotherapy), which present a low efficacy and non-specific toxicity. In this way, the development of innovative therapeutic strategies displaying a higher efficacy and safety is of paramount importance.

Among the therapeutics under study, the Chemo-Photothermal Therapy (Chemo-PTT) mediated by nanomaterials has been showing promising results. This therapeutic modality explores the possible synergistic effects occurring between the nanomaterials mediated' Near Infrared (NIR) light induced heating, as well as its drug delivery capacity. However, less than 1 % of nanoparticles become accumulated within tumor, after systemic administration. To address this limitation, the delivery of nanomaterials directly into the tumor site by injectable tridimensional polymeric matrices has recently started to be explored.

In this MSc Dissertation, an injectable *in situ* forming ionotropically crosslinked chitosan-based hydrogel was developed. Then, Bovine Serum Albumin nanoparticles loaded with IR780 (photothermal agent; IR/BPN) and nanoparticles of D-α-Tocopheryl Polyethylene Glycol 1000 Succinate encapsulating Doxorubicin (chemotherapeutic agent; DOX/TPN) were incorporated within the hydrogel polymeric matrix in order to explore it in cancer Chemo-PTT. The results obtained reveal that the produced hydrogels (IR/BPN@Gel and IR/BPN+DOX/TPN@Gel) present suitable physicochemical properties to be used in cancer therapy. Upon NIR light exposure, the IR/BPN@Gel and IR/BPN+DOX/TPN@Gel produced a temperature increase of 9.2 °C and 9.0 °C, respectively, confirming their photothermal capacity. As importantly, the NIR-light exposure also increased the release of DOX from the hydrogel by 1.7 times.

In the *in vitro* studies, the IR/BPN@Gel presented a cytocompatible behavior towards breast cancer and normal cells. Moreover, the combination of IR/BPN@Gel with NIR light (photothermal therapy) led to a 65 % reduction in the viability of breast cancer cells. On the other hand, the non-irradiated IR/BPN+DOX/TPN@Gel (chemotherapy) only diminished cancer cells viability by 15 %. In stark contrast, the Chemo-PTT mediated by IR/BPN+DOX/TPN@Gel reduced the cancer cells viability by about 91 %. Overall, these

results demonstrate that IR/BPN+DOX/TPN@Gel is an injectable *in situ* forming hydrogel with great potential for the Chemo-PTT of breast cancer.

Keywords

Cancer, Chemo-Photothermal Therapy, Doxorubicin, Injectable Hydrogel, IR780, Localized Delivery.

List of Publications

Articles Published in International Peer Reviewed Journals:

Mó, I.*, Sabino, I. J.*, de Melo-Diogo, D.*, Lima-Sousa, R., Alves, C. G., Correia, I. J.; *The importance of spheroids in analyzing nanomedicines efficacy*, Nanomedicine, 2020. 15 (15), p: 1513–1525. DOI: 10.2217/nnm-2020-0054

* These authors contributed equally to this article.

Index

Figure Index

List of Abbreviations

ANOVA	Analysis of Variance
BPN	BSA Polymeric Nanoparticles
BSA	Bovine Serum Albumin
Chemo-PTT	Chemo-Photothermal Therapy
DMEM-F12	Dulbecco's Modified Eagle's Medium-F12
DOX	Doxorubicin
DOX/TPN	DOX loaded TPGS Polymeric Nanoparticles
DTT	DL-dithiothreitol
EE	Encapsulation Efficiency
FBS	Fetal Bovine Serum
Gel	Chitosan-based Hydrogel incorporating BPN
IR/BPN	IR780 loaded BSA Polymeric Nanoparticles
IR/BPN@Gel	Chitosan-based Hydrogel incorporating IR/BPN
IR/BPN+DOX/TPN@Gel	Chitosan-based Hydrogel incorporating IR/BPN and DOX/TPN
MCF-7	Michigan Cancer Foundation-7
NHDF	Normal Human Dermal Fibroblasts
NIR	Near Infrared
n.s.	non-significant
p53	Tumor Suppressor Protein 53
PBS	Phosphate Buffered Saline
PTT	Photothermal Therapy
SEM	Scanning Electron Microscopy
S.D.	Standard Deviation
TPGS	D-α-Tocopheryl Polyethylene Glycol 1000 Succinate
TPN	TPGS Polymeric Nanoparticles

Chapter 1

Introduction

1. Introduction

1.1. Cancer

Cancer is one of the most prevalent and lethal diseases. The most recent data estimates that cancer will affect 1 806 590 people in the United States of America just in 2020, and that it will cause 606 520 deaths [1]. In Portugal, this disease is the second main cause of death, and its incidence is growing 3 % *per* year [2].

Cancer is characterized by uncontrolled changes in the genetic and epigenetic features of cells, which lead to an abnormal cell growth and proliferation (carcinogenesis) [3, 4]. Hanahan and Weinberg described the Hallmarks of Cancer which include cancer cells' capacity to: a) avoid tumor growth suppressors; b) invade and metastasize healthy tissues; c) develop replicative immortality; d) promote a disorganized angiogenesis; e) resist to cell death mechanisms; f) maintain a proliferative signaling; g) produce abnormal cellular energetics mechanisms; and h) evade immunological destruction (Figure 1) [4].

Malignant cells have autonomy to produce their own growth factors (through autocrine signaling) and to establish interactions with the surrounding cells [4, 5]. Moreover, this type of cells can down-regulate the expression of tumor suppressor genes (*e.g.* tumor suppressor protein 53 (p53) or BRCA1 and BRCA2), hence bypassing proliferation and inhibition mechanisms [5-7].

Cancer cells can also resist to cellular mechanisms that would lead to a controlled death, known as apoptosis [6, 8]. This escape from the programed cell death pathway is guaranteed by different types of regulations [6-8]. In this regard, cancer cells can up-regulate the expression of anti-apoptotic genes (*e.g.* Bcl-2, Bcl-x_L, Bcl-w) and down-regulate the expression of pro-apoptotic ones (*e.g.* Bax and Bak) [6-8].

The replicative immortality characteristic of cancer cells is acquired through the overexpression of telomerase, which is the enzyme responsible for the maintenance of the telomeres length [9]. In this way, these cells can avoid entering into senescence or apoptotic states, further contributing to their proliferation [4, 9].

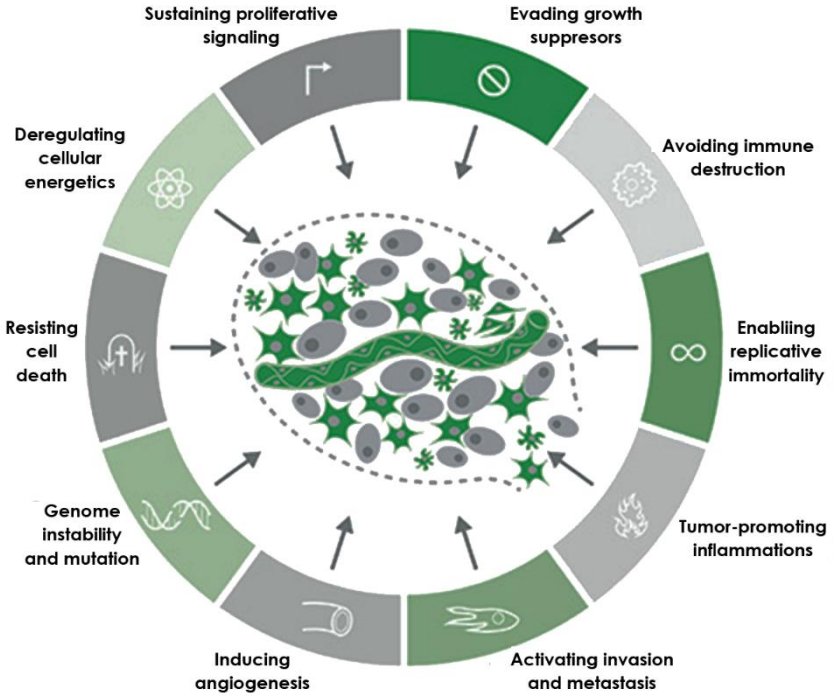

Figure 1 – The Hallmarks of Cancer proposed by Hanahan and Weinberg: a) avoidance of tumor suppressor genes; b) capacity to avoid destruction by the immune system; c) limitless replication; d) invasive capacity; e) unmanageable angiogenesis; f) resistance to cell death mechanisms; g) deregulated cellular energetics; and h) maintenance of a proliferative signaling. The genome instability and mutations as well as tumor-promoting inflammation are the facilitators for the acquisition of these hallmarks (Adapted from [10]).

Furthermore, tumor development is intrinsically dependent on the vasculature, which allows the supply of nutrients and oxygen, and also ensures the removal of metabolites and carbon dioxide [11]. Cancer cells can stimulate the development of new vasculature (angiogenesis), which is crucial for tumor mass growth [4, 11]. However, this process has associated some structural and functional failures (*e.g.* abnormal fenestration diameter), that enable cancer cells to migrate to other tissues as well as the establishment of metastasis [4, 12-14]. Cancer cells' migration is supported by their i) intrinsic characteristics (*e.g.* high malleability, ability to colonize, and adapt to new biological microenvironments) [13], ii) downregulation of cell adhesion molecules (*e.g.* E-cadherin), and iii) upregulation of proteins responsible for cell migration (*e.g.* N-cadherin) [12].

More recently, two new cancer hallmarks were established: deregulation of cellular energetics mechanisms, and avoidance of cancer cells destruction through the immune system [4]. Usually, cancer cells' metabolism is based on the Warburg effect [4, 14]. This energetic pathway is associated with i) large scale conversion of pyruvate into lactate, and ii) high activity levels of oncogenes (*e.g.* RAS and MYC), and low activity levels of tumor suppressor genes (*e.g.* p53) [4, 14]. On the other hand, the immune system is a key defensive element against tumor development and proliferation [15]. Cancer cells have the ability to modify and reprogram immune cells, thus ensuring survival against the immunological defensive system [4, 15].

1.2. Breast cancer

Breast cancer occurs when the main cells in the breast ducts (luminal, epithelial, and myoepithelial cells) are genetically or phenotypically altered [16]. This type of cancer affects mostly women. In 2019, the American Cancer Society estimated that 41 760 deaths occurred as a consequence of breast cancer and that 268 600 new cases were diagnosed [17]. In Portugal, the *Liga Portuguesa Contra o Cancro* estimates that about 6 000 new cases of breast cancer are diagnosed each year [18]. Moreover, it is also estimated that four Portuguese women die daily due to breast cancer [18].

The breast cancer risk factors are related to the age (*e.g.* greater susceptibility of women with more than 50 years), hormone levels (*e.g.* there is an increased predisposition in women who use oral contraceptives), genetic factors (*e.g.* mutations in BRCA1 and BRCA2, or the existence of a family history), and daily routines (*e.g.* a lifestyle based on alcohol consumption, poor physical activity) [19, 20].

A normal and healthy breast epithelium is formed by luminal cells, which are involved in milk formation, and an outer layer of myoepithelial cells that regulate the milk ejection [21]. However, the occurrence of genetic/epigenetic changes may lead to the appearance of aberrant breast cells (Figure 2) [22]. These modifications will also promote the reduction of myoepithelial cells, the destruction of basement membrane, and an augmented presence of infiltrated leukocytes and stromal cells (*e.g.* fibroblasts, myofibroblasts, leucocytes, and endothelial cells) [23]. Then, these cells will evolve to a higher and deregulated proliferative state that will result in an *in situ* carcinoma [21, 23]. The development of an invasive carcinoma is sustained by the secretion of cytokines, chemokines, matrix metalloproteinases or growth factors [23]. Furthermore, breast cancer cells can also interact with: a) cancer associated fibroblasts that can promote the breast cancer cells' progression and auto-renewal [24], b) tumor-associated macrophages that improve cancer development [24], and c) circulating cancer cells which are typically present in blood or lymphatic circulation and may increase the possibility of metastization to healthy tissues [25]. All these interactions contribute to breast cancer heterogeneity [24-26].

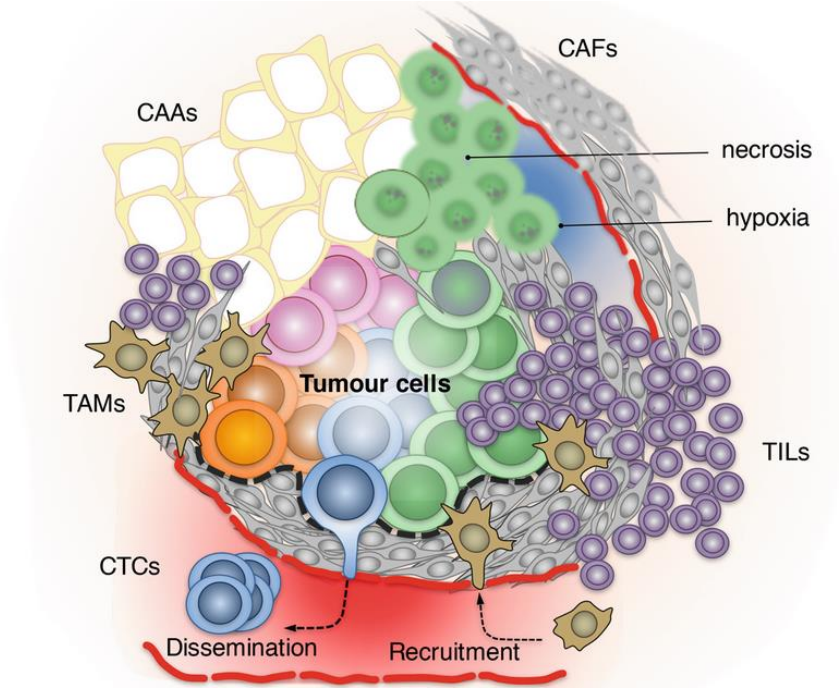

Figure 2 – Schematic representation of the breast tumor microenvironment and of the cells involved in the tumorigenesis process (*e.g.* cancer associated fibroblasts (CAF) and cancer associated adipocytes (CAA)), immune cells (leukocytes and tumor-associated macrophages (TAM)). During cancer growth and development, circulating tumor cells (CTC) can be formed and may be responsible for the metastization process (Adapted from [25]).

Nowadays, breast cancer is commonly treated through surgery (in early stages without metastases) or through the use of chemotherapeutic drugs (chemotherapy) or high energetical radiation (radiotherapy) to ablate tumors at a more advanced stage [16, 27]. Unfortunately, the single or combined use of these therapies induces a suboptimal anticancer effect [28]. Moreover, these therapies also provoke severe side effects, since they affect not only the cancer but also healthy cells [28]. Therefore, it is of great importance to develop effective and safer approaches for breast cancer treatment.

1.3. Cancer combinatorial therapy mediated by nanomaterials

The conventional therapeutic modalities for cancer present several limitations, such as i) lack of efficacy and selectivity towards the cancer cells, ii) solubility problems of chemotherapeutic drugs, and iii) high levels of non-specific radiation-induced toxicity [29-31]. Furthermore, cancer cells can develop resistance mechanisms to chemo and radiotherapies (*e.g.* overexpression of drug efflux pumps, increased levels of DNA repair) that further decrease their efficacy [29, 32].

To overcome this lack of efficacy and bypass the resistance mechanisms, the combination of two or more therapies has been proposed [30, 33]. In this way, combinatorial approaches have the

potential to induce a synergistic therapeutic effect [30, 33, 34]. However, there is a great risk of escalating the already nefarious side effects [30, 35].

To reduce the side effects prompted by the combinatorial therapies, researchers have been developing nanomaterials for achieving a spatio-temporal controlled therapeutic effect [30, 36]. Nanomaterials, due to their dimensions, have the ability to extravasate through the tumor vasculature's fenestrae (dimensions between 200 and 1200 nm), achieving tumor accumulation [37]. Moreover, the impaired lymphatic drainage at the tumor site leads to nanoparticles' retention in this zone. These two factors are known as the Enhanced Permeability and Retention effect [38-40].

Considering the size of the tumor vessels' fenestrae, and taking into account that nanomaterials can also be cleared by the kidneys (for those with a size inferior to 5 nm) or accumulate in the liver and spleen (for those with a size inferior to 50 or greater than 200 nm), nanomaterials' size must be comprehended between 50 and 200 nm in order to achieve a high tumor accumulation [37]. There are other nanoparticles' features that influence their performance [40]. Nanoparticles' charge must be neutral (zeta potential between -10 and +10 mV) since highly negatively or positively charged nanomaterials can have a greater uptake by the reticuloendothelial system cells and the liver, resulting in a decreased tumor accumulation [37, 40]. Furthermore, nanomaterials' surface composition also have a key role in their biological performance [41-43]. Nanomaterials' surface can be modified with hydrophilic components (*e.g.* poly(ethylene glycol) [42] or zwitterionic brushes [41]), which will increase nanomaterials' blood circulation time and hence their tumor uptake [40-42]. On the other hand, the nanostructures' surface can also be decorated with targeting agents (*e.g.* anti-CD44 antibodies [44] or arginine-glycine-aspartic acid conjugate [45]), which will increase their selectivity towards cancer cells [37, 44, 45].

The ability of nanomaterials to incorporate different types of molecules on their structure has propelled their use in combinatorial therapy [43, 46, 47]. For instance, nanomaterials can encapsulate simultaneously different chemotherapeutics in their core, enabling their use for combination chemotherapy [46, 48-50]. Tiwari *et al.* demonstrated that graphene oxide nanomaterials loaded with quercetin and gefitinib (10 mg L^{-1}) could reduce cells' viability to 43 % [48]. On the other hand, nanomaterials loaded with only quercetin or with only gefitinib (both at 10 mg L^{-1}) could only reduce cells' viability to 61 and 62 %, respectively [48].

Moreover, nanostructures with cationic segments and a hydrophobic core can incorporate genetic material (*e.g.* pDNA encoding for p53) and drugs, for being applied in cancer chemo-gene delivery [47, 51]. Ghaffari and co-workers produced poly(amidoamine) dendrimers incorporating curcumin and Bcl-2 siRNA, whose effect reduced cancer cells' viability to 5 % [51]. On the other hand, the single gene delivery or chemotherapy just diminished cancer cells' viability to about 78 and 18 %, respectively [51].

On the other hand, the physicochemical and optical properties of some nanomaterials endow them with loading and photothermal capabilities, thus being explored for chemo-photothermal therapy (Chemo-PTT) [43, 52] – discussed in the next section.

1.4. Combinatorial Chemo-PTT mediated by nanomaterials

Cancer Chemo-PTT has been demonstrating promising results in cancer treatment [53-57]. In general, this therapeutic modality employs nanostructures that can, simultaneously, load chemotherapeutics and perform photothermal heating upon Near Infrared (NIR; 750-1000 nm) laser irradiation [37, 58]. These can be based on inorganic structures, such as gold, copper or carbon-based nanomaterials [59-61]. On the other hand, nanostructures encapsulating NIR-responsive dyes (*e.g.* Indocyanine Green [62], IR780 [43] or MHI-148 [63]) have also been extensively investigated. Alternatively, nanomaterials' mediated Chemo-PTT can also be achieved by administrating one nanostructure that loads the chemotherapeutic drug and another that has photothermal capacity [64-66]. This later approach is more straightforward since it is easier to optimize the physicochemical properties (*e.g.* size) of nanostructures with only one functionality [64-66].

In nanomaterials' mediated Chemo-PTT, the use of NIR radiation is of extreme importance since it presents a high penetration depth and low interaction with biological components, such as water, melanin, hemoglobin or collagen (Figure 3) [40, 67].

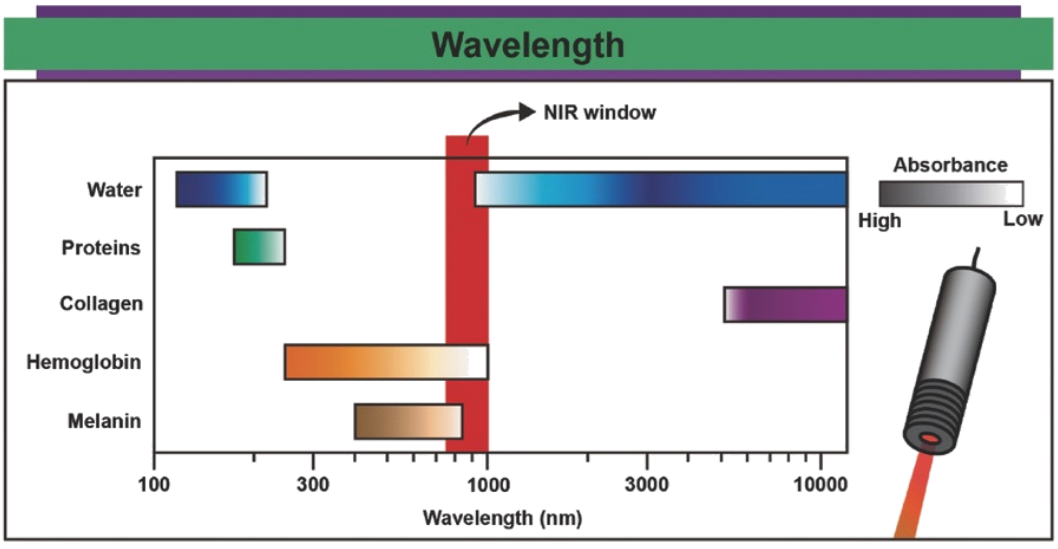

Figure 3 – Schematic representation of the absorption of the major human body components, at different wavelengths. The main constituents of the human body (*e.g.* water, proteins, collagen, hemoglobin, and melanin) do not interact significantly with radiation with wavelengths in the 750-1000 nm (NIR region). Thereby, the use of NIR light in PTT enables a high penetration depth and minimal off-target heating (Adapted from [40]).

After nanomaterials reach the tumor microenvironment, the tumor zone is irradiated with NIR light [40, 68, 69]. Then, the nanomaterials absorb this energy and release it as heat [40, 68, 69]. A hyperthermia to 41-45 °C can induce alterations in the metabolic functions of cells, inhibit DNA repair mechanism, and create reactive oxygen species [37, 38]. Furthermore, a hyperthermia to above 50 °C severely affects cellular functions (*e.g*. dysfunction of mitochondrial and enzymatic functions, proteins' denaturation and collapse), and ultimately leads to cells' death by necrosis [39, 40].

Moreover, the attained temperature increase can enhance the blood circulation in the tumor microenvironment, ultimately augmenting the number of nanoparticles that can reach the tumor site [58]. Furthermore, it can also enhance nanomaterials' internalization by affecting the cell membranes' permeability [58, 70]. As importantly, the nanomaterials' mediated photoinduced heat can also trigger the release of the chemotherapeutics from the nanostructures and/or sensitize cells to the action of chemotherapeutics drugs, leading to an improved therapeutic effect [43, 70]. Additionally, the temperature increase can also trigger the rupture of the endosomes, preventing the degradation of the chemotherapeutics in these vesicles [58, 70].

By taking advantage of these phenomena, the Chemo-PTT mediated by nanomaterials can lead to an improved therapeutic outcome using lower drug doses and/or using weaker irradiation intensities [71, 72]. Despite the potential of nanomaterials mediated Chemo-PTT, a recent report just demonstrated that the median of the nanoparticles' dose accumulated at the tumor site after intravenous injection is below 1 % [73]. Moreover, for nanomaterials aimed for Chemo-PTT to achieve a tumor uptake concomitant with tumor eradication, it is necessary to exhaustively optimize the nanomaterials' physicochemical properties (*e.g*. size, surface composition) [35, 40, 58, 70]. In this way, it is of extreme importance to develop innovative strategies to deliver nanomaterials directly into the tumor site, hence improving their Chemo-PTT potential.

1.5. Injectable *in situ* forming hydrogels

To overcome the issues associated with the intravenous administration of nanoparticles, localized delivering strategies have been receiving a growing attention (Figure 4) [74, 75]. Over the years, different types of strategies have been developed for the intratumoral delivery of nanomaterials [76], such as microneedles [52], microdevices [77] or hydrogels [53].

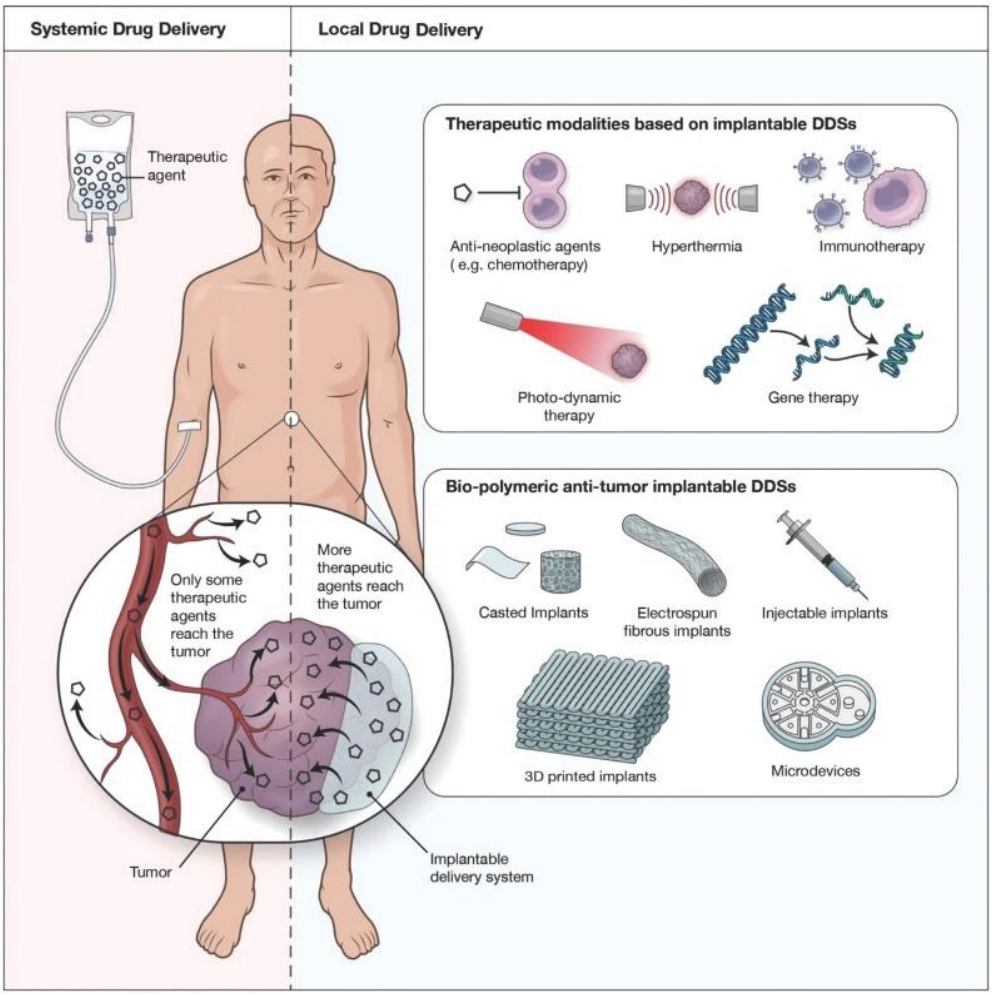

Figure 4 – Schematic comparison of systemic *vs*. local drug delivery strategies for the treatment of superficial cancers (Adapted from [75]).

Recently, the use of injectable *in situ* forming hydrogels for delivering nanomaterials aimed for cancer Chemo-PTT has been showing promising results [53, 78-80]. The *in situ* gelation of these hydrogels enables the administration of the nanomaterials without discomfort to the patient, using a minimally invasive procedure [75, 76, 81, 82]. Furthermore, the *in situ* formed hydrogels confine the nanomaterials in the tumor zone, diminishing their leakage to off-target tissues [81-84]. As importantly, the nanomaterials are sustainably released from the hydrogel into the tumor tissue, leading to a controlled effect [84].

To prepare injectable *in situ* forming hydrogels, the nanomaterials are initially dispersed in an aqueous polymeric solution [74, 84, 85]. For this purpose, natural-based polymers (*e.g*. chitosan, collagen or alginate) are usually used, since these ensure an adequate biocompatibility and biodegradability of the hydrogels [76, 81, 83].

Then, after intratumoral injection, the hydrogels form *in situ* [53, 74, 75, 82, 86-88]. The *in situ* gelification of these hydrogels can be achieved by different mechanisms, being the thermo-responsive gelation and the electrostatic or covalent crosslinking the most commonly explored (Figure 5) [76, 81].

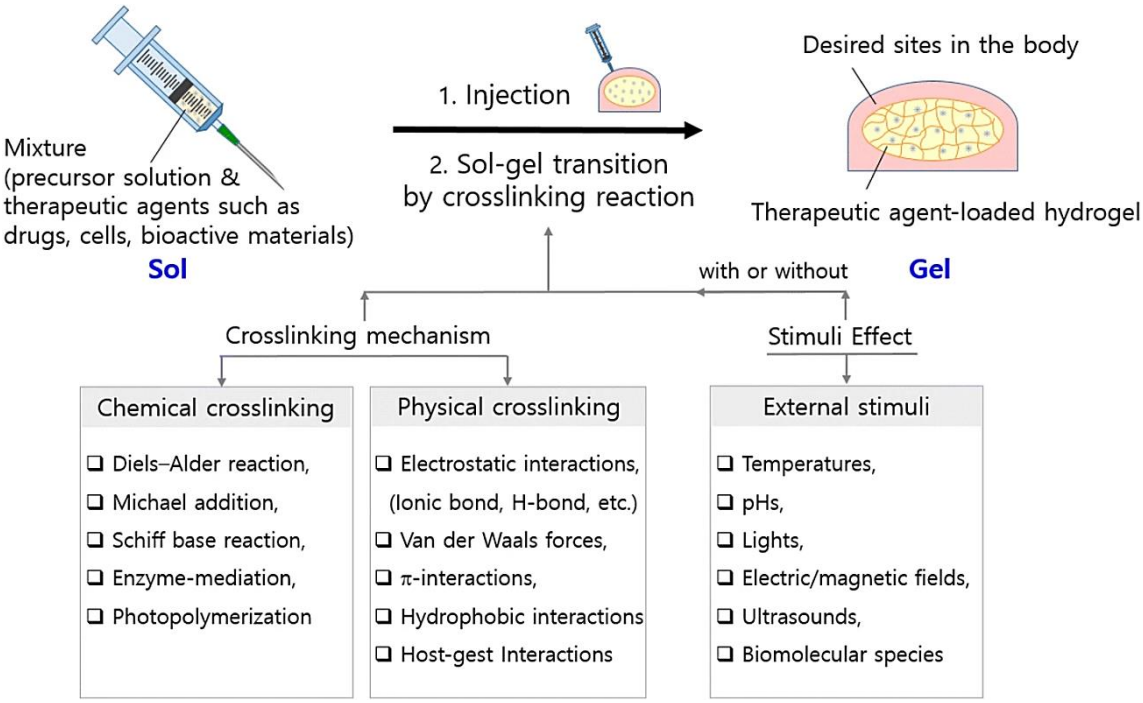

Figure 5 – Schematic representation of the formation of injectable hydrogels loading therapeutic agents, through physical or chemical-based crosslinking interactions with or without external stimuli (Adapted from [81]).

Lima-Sousa *et al.* produced injectable *in situ* forming thermo-responsive chitosan-agarose hydrogels containing reduced graphene oxide (photothermal nanoagent) and loading a Doxorubicin (DOX):Ibuprofen combination for cancer Chemo-PTT [53]. In *in vitro* studies, the Chemo-PTT mediated by this hydrogel (90.4 μM of the drug combination; 808 nm, 1.7 W cm^{-2}, 10 min) could reduce cancer cells' viability to 34 % [53]. In contrast, the hydrogels' mediated PTT and hydrogels' induced chemotherapy only reduced cells viability to 60 and 75 %, respectively [53]. In another work, Zheng and colleagues developed a thermo-responsive injectable chitosan-based hydrogel incorporating molybdenum nanosheets and DOX [89]. *In vivo*, the hydrogels' mediated Chemo-PTT (808 nm, 1 W cm^{-2}, 5 min) induced a greater reduction on tumor's growth than the hydrogels that solely performed one therapeutic modality [89]. Zhao *et al.* produced alginate-based hydrogels electrostatically crosslinked with Ca^{2+} that incorporated poly(pyrrole) (photothermal agent) and DOX [90]. The *in vitro* assays demonstrated that the Chemo-PTT mediated by this hydrogel (808 nm, 0.5 W cm^{-2}, 5 min) was able to reduce cancer cells' viability to approximately 14 %. In contrast, the PTT or chemotherapy mediated by the hydrogels only reduced the cells' viability to 27 and 30 %, respectively [90].

Among these, injectable *in situ* forming hydrogels assembled using electrostatic interactions have gathered a great interest due to their ease of preparation – reviewed in the next section.

1.6. Engineering injectable *in situ* forming hydrogel for Chemo-PTT

Injectable *in situ* forming hydrogels assembled using electrostatic interactions hold a great potential for the tumor-confined delivery of nanomaterials aimed for Chemo-PTT. This type of hydrogel can be prepared using two or more polymers with alternating charge (*e.g.* chitosan plus poly(vinyl alcohol)) [91]. Alternatively, these can also be assembled by the ionotropic crosslinking of polymeric structures (*e.g.* alginate plus Ca^{2+}) [92]. Among the different polymers that could be used to prepare these hydrogels, chitosan is an appealing one due to its ease of crosslinking with HCO_3^- and OH^- [91, 93]. Moreover, chitosan is also biocompatible and biodegradable [86, 94, 95]. Chitosan also has antibacterial properties, which can be useful in minimal invasive procedures that still have some risk of infection [94, 95].

In this way, the preparation of injectable *in situ* forming chitosan hydrogels through ionotropic crosslink with $NaHCO_3$ for delivering nanomaterials aimed for cancer Chemo-PTT appears to be a promising approach. In this regard, the loading of IR780 (a hydrophobic NIR-responsive small molecule) into Bovine Serum Albumin (BSA) nanoparticles and their incorporation in the hydrogels can be performed to endow the hydrogels with photothermal capacity. The selection of BSA nanoparticles to incorporate IR780 is related with their good loading capacity and biocompatibility [96]. On the other hand, D-α-Tocopheryl Polyethylene Glycol 1000 Succinate (TPGS) can be used to prepare nanoparticles incorporating DOX. Besides the TPGS self-assembling capacity, this molecule is also capable of inhibiting P-glycoprotein (a major DOX efflux pump) [97, 98]. The incorporation of DOX loaded TPGS nanoparticles into the chitosan-$NaHCO_3$ injectable *in situ* forming hydrogels confers it a chemotherapeutic application.

In this way, chitosan-$NaHCO_3$ injectable *in situ* forming hydrogels co-incorporating IR780 loaded BSA nanoparticles and DOX loaded TPGS nanoparticles may be a promising technology for cancer Chemo-PTT.

1.7. Aims

The main objective of this Master Dissertation work plan was to develop an injectable *in situ* forming chitosan-$NaHCO_3$ hydrogel co-incorporating BSA polymeric nanoparticles (BPN) loaded with IR780 (IR/BPN) and TPGS polymeric nanoparticles (TPN) loaded with DOX (DOX/TPN) for application in the Chemo-PTT of breast cancer cells.

The specific aims of this MSc workplan are:

- Development and characterization of IR/BPN and DOX/TPN;
- Formulation of the injectable *in situ* forming chitosan-based hydrogels i) with blank BPN, ii) incorporating IR/BPN, and iii) co-incorporating IR/BPN and DOX/TPN;
- Characterization of the physicochemical properties of the produced hydrogels;
- Determination of the cytocompatibility of chitosan-based hydrogels and of chitosan-based hydrogels incorporating IR/BPN;
- Evaluation of the PTT mediated by chitosan-based hydrogels incorporating IR/BPN towards breast cancer cells;
- Evaluation of the Chemo-PTT mediated by chitosan-based hydrogels co-incorporating IR/BPN and DOX/TPN towards breast cancer cells.

Chapter 2

Experimental Section

2. Experimental Section

2.1. Materials

BSA was bought from Amresco (Pennsylvania, USA). Chitosan low molecular weight (50 000 – 190 000 Da), DL-dithiothreitol (DTT), Dulbecco's Modified Eagle's Medium F12 (DMEM-F12), IR780 iodide, Phosphate Buffered Saline (PBS), resazurin, TPGS, and trypsin were purchased from Sigma-Aldrich (Sintra, Portugal). Acetone, methanol, and $NaHCO_3$ were purchased from Fisher Scientific (Oeiras, Portugal). Cell culture plates and T-flasks were acquired from Thermo Fisher Scientific (Porto, Portugal). DOX was obtained from Carbosynth (Berkshire, UK). Lysozyme from chicken egg was acquired from Alfa Aesar (Haverhill, MA, USA). Fetal Bovine Serum (FBS) was provided by Biochrom AG (Berlin, Germany). Michigan Cancer Foundation-7 (MCF-7) cell line and Normal Human Dermal Fibroblast (NHDF) were obtained from ATCC (Middlesex, UK) and Promocell (Heidelberg, Germany), respectively. Water used in all experiments was double deionized (0.22 μm; 18.2 MΩ cm^{-1}).

2.2. Methods

2.2.1. Formulation of IR/BPN and DOX/TPN

The IR/BPN were prepared by adapting a nanoprecipitation method previously described by Alves *et al.* [99]. Briefly, BSA (5 mg) and DTT (386 μg) were allowed to react for 20 min, under stirring, in 5 mL of PBS. Afterwards, IR780 (250 μg, in 1 mL of acetone) was added dropwise into the BSA-DTT solution, under constant stirring, for 2 h at room temperature. The obtained solution was recovered, dialyzed against water (14 000 Da cut-off membrane) for 90 min, and filtered (0.45 μm pore size), yielding IR/BPN. As control, BPN without IR780 were also produced.

The DOX/TPN were prepared according to the method reported by Pais-Silva *et al.* [100]. Briefly, a mixture of TPGS (5 mg) and DOX (250 μg) in 1 mL of acetone was prepared and it was added dropwise into 5 mL of water, under constant stirring, for 2 h at room temperature. The obtained solution was recovered, dialyzed against water (500 – 1 000 Da cut-off membrane) for 90 min, and filtered (0.45 μm pore size), yielding DOX/TPN.

2.2.2. Physicochemical characterization of IR/BPN and DOX/TPN

The IR/BPN and DOX/TPN size distribution (at a scattering angle of 173°) and zeta potential were evaluated in a Zetasizer Nano ZS (Malvern Instruments Ltd., Worcestershire, UK). The Vis-NIR absorption spectrum of IR/BPN and DOX/TPN was also acquired (Evolution 201 UV–Visible spectrophotometer (Thermo Fisher Scientific Inc., Massachusetts, USA)).

To determine the IR780 content in IR/BPN, these nanoparticles were freeze-dried (ScanVac CoolSafe, Labo-Gene ApS, Lynge, Denmark) and then resuspended in 1 mL of a water:methanol solution (1:1 (v/v)). Afterwards, a standard curve of IR780 (in 1:1 (v/v) water:methanol) and the absorbance of the IR/BPN sample at 780 nm were used to determine the content of IR780. To determine the DOX content in DOX/TPN, these nanoparticles were also freeze-dried and

resuspended in 1 mL of methanol. Then, a standard curve of DOX (in methanol) and the DOX/TPN absorbance at 485 nm were used to assess the DOX content. Then, the encapsulation efficiency (EE) of IR780 in IR/BPN and of DOX in DOX/TPN were determined according to Equation (1):

$$\text{EE}\ (\%) = \frac{\text{Weight of IR780 or DOX encapsulated in the nanoparticles}}{\text{Weight of IR780 or DOX initially fed}} \times 100 \quad (1)$$

2.2.3. Preparation of the ionotropically crosslinked chitosan-based hydrogels

The injectable *in situ* forming ionotropically crosslinked chitosan hydrogel incorporating IR/BPN (IR/BPN@Gel) was prepared by adapting the method described by Wang *et al.* [93]. Firstly, the gelling agent solution was prepared by dissolving $NaHCO_3$ (945 mg) in PBS (0.1 M, 20 mL). Then, the gelling agent solution (200 µL) was mixed with IR/BPN (400 µL; 35 µg mL^{-1} of IR780 equivalents). Afterwards, this solution was added to the chitosan solution (900 µL; 4 % (w/v) in HCl). Subsequently, the gelling agent-IR/BPN-chitosan solution was loaded into a syringe and it was extruded (400 µL *per* template) into hollow cylindrical and removable templates (⌀ = 8 mm; height = 4 mm) in order to attain hydrogels with uniform macroscopic features. This hydrogel formulation was stored at physiological-like conditions (37 °C, 5 % CO_2) before its use.

For the preparation of the IR/BPN+DOX/TPN@Gel, a similar protocol was used, with slight alterations. Briefly, a mixture of the gelling agent (200 µL), IR/BPN (400 µL; 35 µg mL^{-1} of IR780 equivalents) and DOX/TPN (200 µL; 15 µg mL^{-1} of DOX equivalents) was prepared, and added to the chitosan solution (900 µL; 4 % (w/v) in HCl). Then, the gelling agent-IR/BPN-DOX/TPN-chitosan solution was loaded into a syringe and it was extruded (400 µL *per* template) as described above.

As a control, injectable *in situ* forming ionotropically crosslinked chitosan hydrogels were also prepared with blank (non-drug loaded) BPN (termed as Gel).

2.2.4. Characterization of the Gel, IR/BPN@Gel and IR/BPN+DOX/TPN@Gel

The swelling behavior of the hydrogels was determined following a protocol previously described [53]. Briefly, Gel, IR/BPN@Gel and IR/BPN+DOX/TPN@Gel were immersed in a PBS solution (pH 7.4, 1 mL) at 37 °C, under stirring. At predetermined timepoints, the hydrogels were removed from the PBS solution and weighted. Afterwards, they were immersed in a new PBS solution. The swelling ratio was determined using the following equation (W_F and W_I represent the weight of the hydrogels at the determined timepoints and at the beginning, respectively):

$$\text{Swelling Ratio (\%)} = \frac{W_F - W_I}{W_I} \times 100 \quad (2)$$

The degradation of Gel, IR/BPN@Gel and IR/BPN+DOX/TPN@Gel in biologically mimicking conditions was also investigated [101]. For such, each hydrogel was placed in a PBS solution (pH 7.4, 1 mL) containing lysozyme (13.6 mg L^{-1}) at 37 °C, under stirring for 7 days. The PBS-enzyme solution was replaced every 2 days. At predetermined timepoints, the hydrogels were recovered and washed 3 times with water, freeze-dried and then weighted. The weight loss at the determined timepoints was calculated according to the following equation (W_I and W_T represent the hydrogels' initial weight and the hydrogels' weight at time t, respectively):

$$\text{Weight Loss (\%)} = \frac{W_I - W_T}{W_I} \times 100 \quad (3)$$

The photothermal capacity of Gel, IR/BPN@Gel and IR/BPN+DOX/TPN@Gel was also analyzed [43, 53]. For this purpose, the hydrogels were immersed in water and then irradiated with NIR light for 10 min (808 nm, 1.7 W cm^{-2}). At predetermined timepoints, the temperature variations were recorded using a thermocouple thermometer. Water was used as a control.

The cross-section morphology of Gel, IR/BPN@Gel and IR/BPN+DOX/TPN@Gel was observed by Scanning Electron Microscopy (SEM) at an acceleration voltage of 20 kV using a Hitachi S-3400N Scanning Electron Microscope (Japan).

The release profile of DOX from the IR/BPN+DOX/TPN@Gel was determined by placing this formulation in a PBS solution (pH 7.4, 500 µL) containing lysozyme (13.6 mg L^{-1}) at 37 °C [53]. At pre-established timepoints, the PBS-enzyme solution was recovered and replaced by a fresh one. Afterwards, the DOX content in the recovered solutions was determined by absorption spectroscopy. The influence of the NIR light exposure on the release of DOX was also determined by irradiating the hydrogel (808 nm, 1.7 W cm^{-2}, 10 min).

For analyzing the long-term stability of Gel, IR/BPN@Gel and IR/BPN+DOX/TPN@Gel, their respective precursor solutions (described in Section 2.2.3.) were stored at 4 °C during 7 days. Afterwards, the hydrogels were assembled by loading the stored solutions into syringes. Then, the injectability and gelation after storage was evaluated. The size distribution of the IR/BPN and DOX/TPN after storage was also evaluated.

2.2.5. Evaluation of Gel and IR/BPN@Gel cytocompatibility

The cytocompatibility of Gel and IR/BPN@Gel (3.73 μg mL^{-1} of IR780 equivalents) was evaluated on MCF-7 cells (breast cancer cell model) and NHDF (normal cell model) using the resazurin method [102]. For the cell culture assays, both cell lines were cultured in DMEM-F12 supplemented with 10 % (v/v) of FBS and 1 % (v/v) of penicillin/streptomycin, in a humidified incubator (37 °C, 5 % CO_2). Briefly, 2×10^4 cells/well were seeded in 12-well plates. After 24 h, the culture medium was removed, and the cells were incubated with fresh medium and with the Gel or IR/BPN@Gel. After 24 or 48 h of incubation, the hydrogels were removed, and the cells were incubated with fresh culture medium containing resazurin (10 % (v/v)) for 4 h in the dark (37 °C, 5 % CO_2). Then, the fluorescence of resorufin (λ_{ex} = 560 nm; λ_{em} = 590 nm) was measured (Spectramax Gemini EM spectrofluorometer, Molecular Devices LLC, CA, USA) to determine the cells' viability. Cells solely incubated with medium and ethanol (70 % (v/v)) were used as negative (K^-) and positive (K^+) controls, respectively.

2.2.6. *In vitro* evaluation of the PTT mediated by IR/BPN@Gel and of the Chemo-PTT mediated by IR/BPN+DOX/TPN@Gel

The therapeutic effect mediated by IR/BPN@Gel and IR/BPN+DOX/TPN@Gel was determined using the resazurin method as described above [55]. Initially, MCF-7 cells were seeded as described in Section 2.2.5. After 24 h, cells were incubated with fresh medium and with IR/BPN@Gel (3.73 μg mL^{-1} of IR780 equivalents) or IR/BPN+DOX/TPN@Gel (3.29/0.71 μg mL^{-1} of IR780/DOX equivalents). Then, after 4 h of incubation, the hydrogels were irradiated with NIR light (808 nm, 1.7 W cm^{-2}, 10 min). Subsequently, after totalling 24 h of incubation, the cells' viability was evaluated as described in Section 2.2.5.

2.2.7. Statistical Analysis

To compare multiple groups, a one-way Analysis of Variance (ANOVA) with the Student-Newman-Keuls test was used. A value of p lower than 0.05 ($^*p < 0.05$) was considered statistically significant. All data are represented as the mean ± Standard Deviation (S.D.). Data analysis was performed in the GraphPad Prism v6.0 Software (trial version, GraphPad Software, CA, USA).

Chapter 3

Results and Discussion

3. Results and Discussion

3.1. Formulation and characterization of IR/BPN and DOX/TPN

The incorporation of IR/BPN and DOX/TPN in the injectable *in situ* forming ionotropically crosslinked chitosan hydrogel was aimed for application in cancer Chemo-PTT (Figure 6).

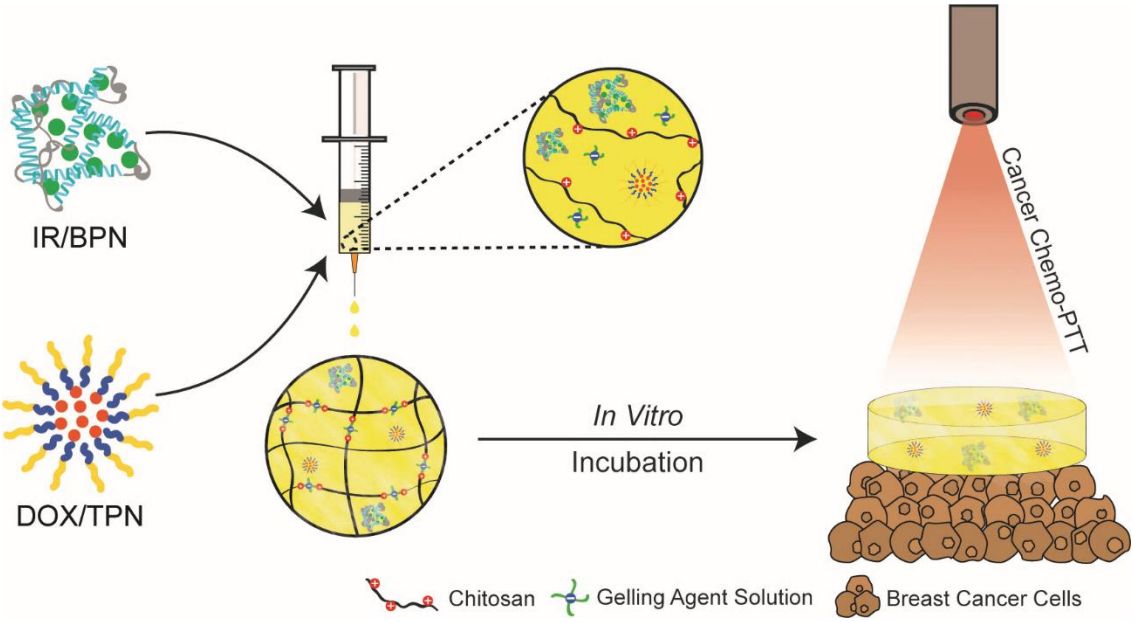

Figure 6 – Schematic representation of the formulation of the injectable *in situ* forming ionotropically crosslinked chitosan hydrogel loaded with IR/BPN and DOX/TPN and of its application in Chemo-PTT of breast cancer cells.

To accomplish that, IR/BPN and DOX/TPN were initially prepared using a nanoprecipitation method. The Dynamic Light Scattering analysis demonstrated that IR/BPN presented an average size of 89.4 ± 1.0 nm (n = 3; batch triplicates; Figure 7) while the DOX/TPN showed a size of 56.3 ± 0.5 nm (n = 3; batch triplicates; Figure 7). The smaller size of DOX/TPN is related with the ability of TPGS to assemble into very small nanostructures [103]. Nevertheless, the size of both IR/BPN and DOX/TPN is within the dimensions considered as ideal for cancer related applications [104-106]. For instance, Stern *et al.* demonstrated that nanoparticles with a mean size of 50-90 nm have a good penetration into 3D tumor-like cellular aggregates, as well as a suitable uptake by cancer cells [105].

The zeta potential of IR/BPN and DOX/TPN were -4.8 ± 0.5 mV and -4.1 ± 0.5 mV, respectively. In this way, these nanoformulations have a surface charge within the so-called neutral surface charge range (zeta potential between -10 and +10 mV), which has been considered as optimal for tumor penetration [40]. Furthermore, the surface charge of IR/BPN and DOX/TPN is also in line with that reported in the literature for BSA-based and TPGS-based nanomedicines [107, 108].

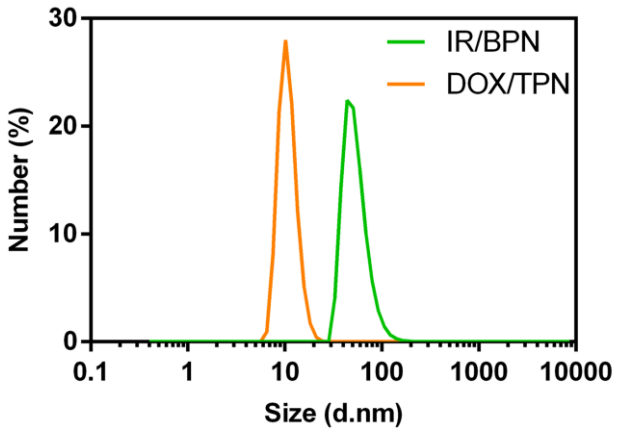

Figure 7 – Dynamic Light Scattering size distribution of IR/BPN and DOX/TPN.

Moreover, the absorption of IR/BPN and DOX/TPN was analyzed (Figure 8). As expected, the IR/BPN and DOX/TPN exhibited the characteristic peaks for IR780 and DOX, respectively. The IR/BPN displayed an IR780 encapsulation efficiency of 70 %. On the other hand, the DOX/TPN encapsulated DOX with an efficiency of about 45 %. The lower encapsulation capacity of DOX/TPN may be related with their smaller sized hydrophobic core [103]. Nevertheless, these encapsulation results are in agreement with those of other BSA and TPGS-based nanoparticles [109, 110].

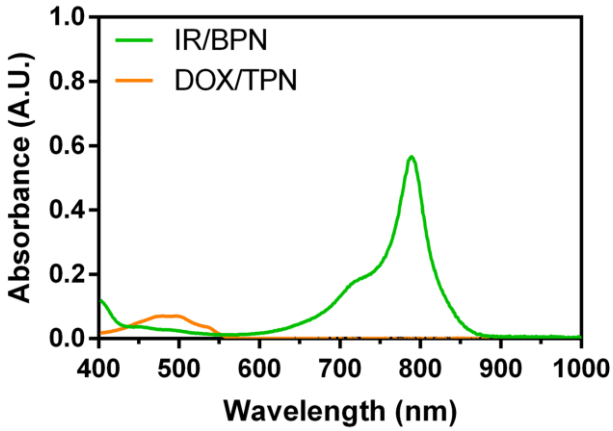

Figure 8 – Absorption spectra of IR/BPN (3.0 μg mL^{-1} of IR780; in water) and DOX/TPN (3.0 μg mL^{-1} of DOX; in water).

3.2. Preparation and characterization of Gel, IR/BPN@Gel and IR/BPN+DOX/TPN@Gel

After the preparation of IR/BPN and DOX/TPN, these nanoformulations were added to chitosan and $NaHCO_3$, for the assembly of the injectable *in situ* forming ionotropically crosslinked hydrogels with chemo-photothermal capacity. For such, a mixture of IR/BPN, DOX/TPN, $NaHCO_3$, and chitosan was loaded into a syringe and was injected into hollow cylindrical and removable templates. Such led to the assembly of individual IR/BPN+DOX/TPN@Gel with uniform macroscopic characteristics for the subsequent assays (Figure 9).

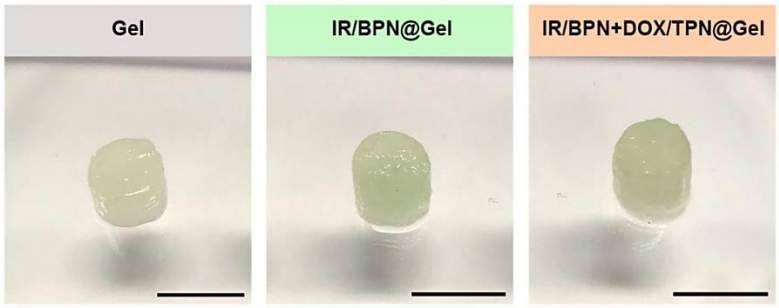

Figure 9 – Macroscopic images of Gel, IR/BPN@Gel and IR/BPN+DOX/TPN@Gel. Scale bars represent 1 cm.

Hydrogels incorporating only IR/BPN were also prepared using the same procedure (termed as IR/BPN@Gel). As a control, hydrogels with blank (non-loaded) BPN were also produced (termed as Gel). All the three different formulations displayed consistent macroscopic characteristics (Figure 9) and an irregular-interconnected porous inner structure (Figure 10). Compared to Gel, the IR/BPN@Gel and IR/BPN+DOX/TPN@Gel displayed a more cohesively packed inner structure, which could result from the ability of the nanoparticles to establish interactions with the hydrogels' polymeric network [38, 82].

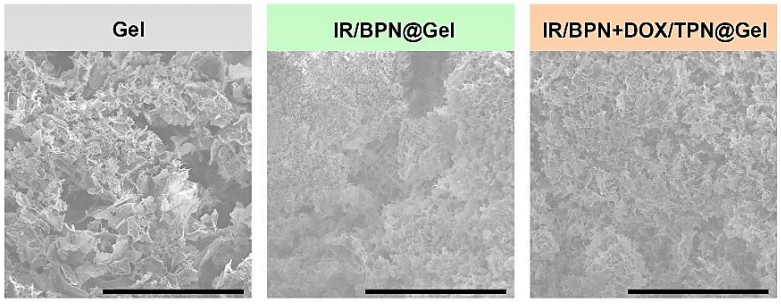

Figure 10 – SEM images of the cross-section of Gel, IR/BPN@Gel and IR/BPN+DOX/TPN@Gel. Scale bars represent 1 mm.

The swelling behavior of the different hydrogels was also investigated (Figure 11). The three formulations exhibited similar swelling profiles, reaching a maximum swelling of about 13 % after 24 h of incubation (Figure 11). The slow swelling exhibited by these hydrogels is of utmost importance since an abrupt and high swelling profile would compromise the future application on these hydrogels inside tumoral mass [111].

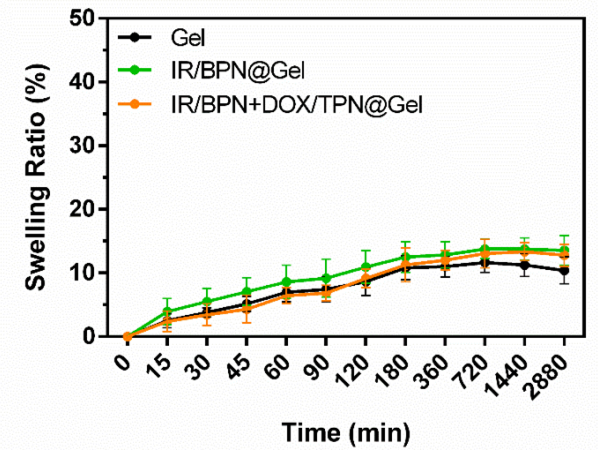

Figure 11 – Assessment of the swelling behavior of the hydrogels for a period of 48 h. Data represents mean ± S.D., n = 5.

Then, the hydrogels' degradability in biologically mimicking conditions was analyzed (Figure 12). In general, all hydrogel formulations displayed an initial weight loss of 17 % after 1 day of incubation. The Gel formulation achieved its maximum weight loss of about 24 %, after 3 days of incubation (Figure 12). In stark contrast, both IR/BPN@Gel and IR/BPN+DOX/TPN@Gel displayed an incubation time-dependent weight loss, having their mass decreased by about 48 % by day 7 (Figure 12). In this way, the sustained degradability of IR/BPN@Gel and IR/BPN+DOX/TPN@Gel may enable a controlled release of the different nanoformulations.

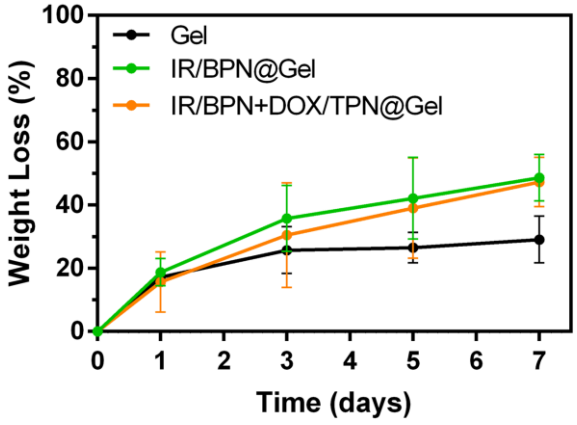

Figure 12 – Evaluation of hydrogels' weight loss in biologically mimicking conditions, over a period of 7 days. Data represents mean ± S.D., n = 5.

Afterwards, the photothermal capacity of the hydrogels was assessed by exposing them to NIR radiation during a period of 10 min (808 nm, 1.7 W cm^{-2}) – Figure 13. The IR/BPN@Gel and IR/BPN+DOX/TPN@Gel produced an irradiation time-dependent photoinduced heat. After 10 min of NIR laser irradiation, the IR/BPN@Gel (3.73 μg mL^{-1} of IR780 equivalents) and IR/BPN+DOX/TPN@Gel (3.29 μg mL^{-1} of IR780 equivalents) produced a temperature increase of 9.2 °C and 9.0 °C, respectively (Figure 13). The photothermal capacity of these hydrogels is related with the presence of IR/BPN in their structure [99]. As importantly, such temperature increase can cause damage to cells, leading to a therapeutic effect [112, 113]. As expected, the irradiation of Gel with NIR light did not cause a meaningful temperature variation since this formulation does not have any photothermal nanoagent within its matrix (Figure 13). Similarly, water (control) exposed to NIR light also did not suffer any significant temperature variation, which is in concordance with its weak/minimal interaction with 808 nm light [40]. As importantly, the NIR laser irradiation also increased the DOX release from the IR/BPN+DOX/TPN@Gel by up to 1.7-fold (Figure 14). In this way, IR/BPN+DOX/TPN@Gel may be able to promote an on-demand spatio-temporal controlled cancer therapeutic effect.

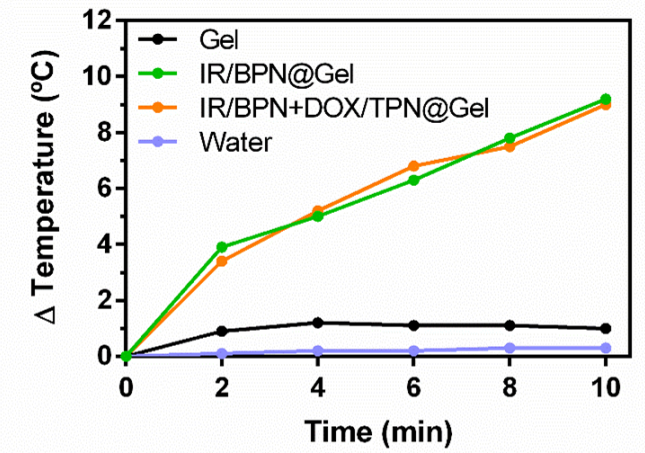

Figure 13 – Temperature variation curves of the different hydrogel formulations upon NIR laser irradiation (808 nm, 1.7 W cm^{-2}, 10 min).

Wang *et al.* developed alginate-based hydrogel incorporating iodine-starch complexes (1 mg mL^{-1}) that produced a temperature increase of 19.4 °C after NIR light exposure (808 nm, 2.0 W cm^{-2}, 10 min) [112]. In another work, Lima-Sousa *et al.* verified that chitosan-agarose hydrogels incorporating reduced graphene oxide produce a photoinduced heat of 8.1 °C (10 μg mL^{-1}; 808 nm, 1.7 W cm^{-2}, 10 min) [53]. Herein, the IR/BPN+DOX/TPN@Gel was able to induce a temperature increase of 9.0 °C using a lower dose of photothermal nanoagent (3.29 μg mL^{-1} of IR780 equivalents) and using a lower/similar NIR radiation intensity (1.7 W cm^{-2}). These findings attest the good photothermal capacity of IR/BPN+DOX/TPN@Gel.

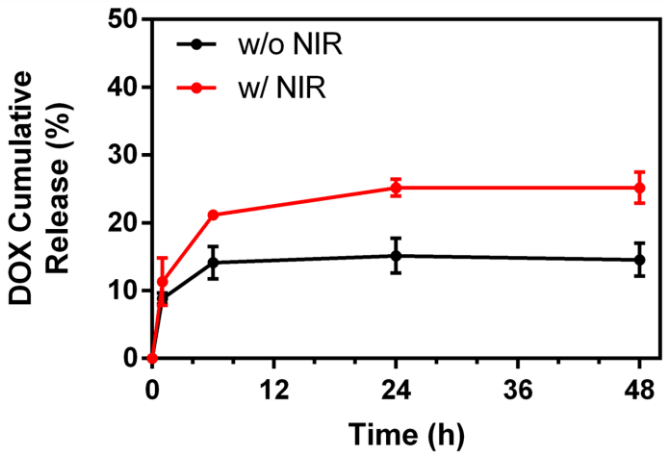

Figure 14 – Cumulative Release of DOX from IR/BPN+DOX/TPN@Gel during a 48 h period without (w/o NIR) and with (w/ NIR) NIR laser irradiation (808 nm, 1.7 W cm^{-2}, 10 min). Data represents mean ± S.D., n = 3.

Finally, the long-term stability of the different hydrogels was evaluated. After 7 days of storage at 4 °C, the IR/BPN and DOX/TPN did not suffer any aggregation and thus retained most of their original size distribution (Figure 15). Furthermore, by loading the stored nanoformulations and the stored hydrogels' precursor solutions ($NaHCO_3$ and chitosan solutions) into a syringe, the injectability and gelation of the different hydrogels were still achieved (Figure 16), thus demonstrating a good stability.

Taken together, these results demonstrate the good physicochemical and optical properties of IR/BPN@Gel and IR/BPN+DOX/TPN@Gel.

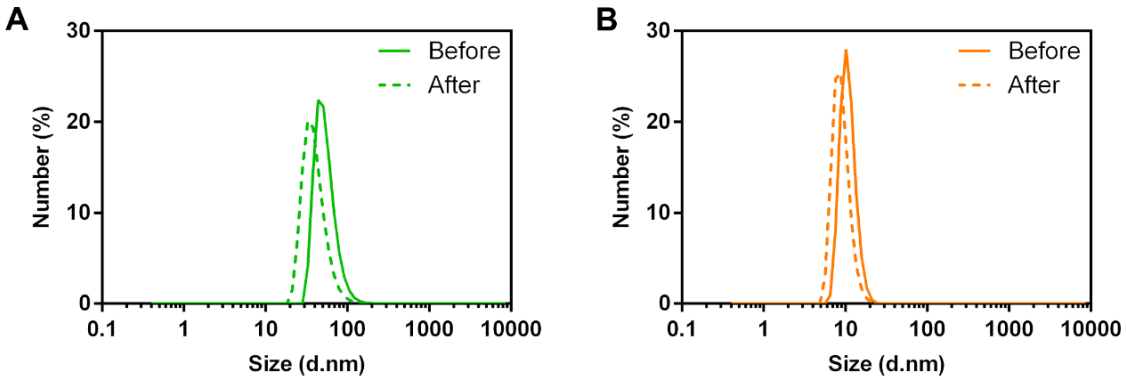

Figure 15 – Dynamic Light Scattering size distribution of IR/BPN (A) and DOX/TPN (B) before and after storage for 7 days at 4 °C.

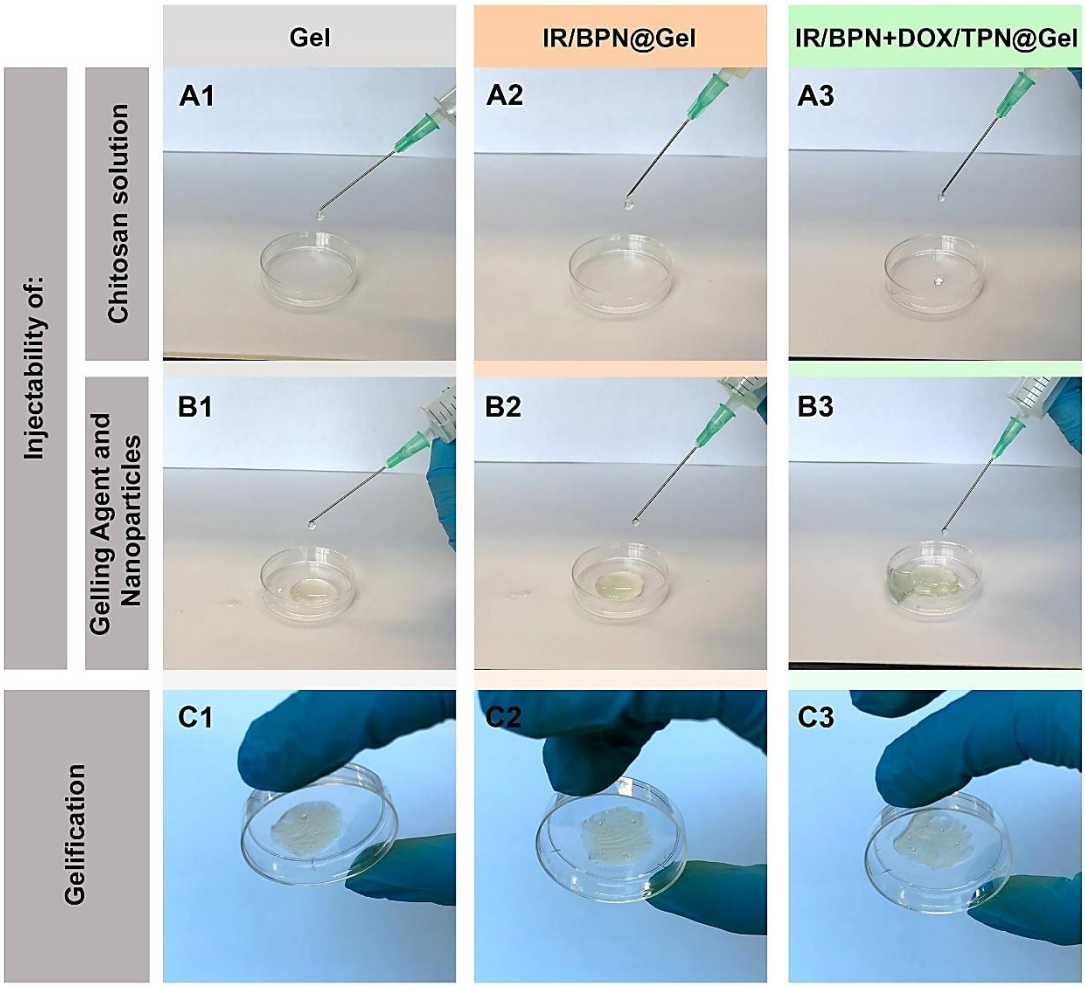

Figure 16 – Long-term stability of the hydrogels. Macroscopic images of the extrusion of the chitosan (A1-A3) and gelling agent/nanoparticles solutions (B1-B3) after storage for 7 days at 4 °C required for the assembly of Gel (A1, B1), IR/BPN@Gel (A2, B2), and IR/BPN+DOX/TPN@Gel (A3, B3). Macroscopic images of the gelification of Gel (C1), IR/BPN@Gel (C2), and IR/BPN+DOX/TPN@Gel (C3), using the stored components, as confirmed by the inversion test.

3.3. Evaluation of Gel and IR/BPN@Gel cytocompatibility

Then, the cytocompatibility of the Gel and IR/BPN@Gel towards MCF-7 cells and NHDF was assessed (Figure 17). Both hydrogel formulations revealed a cytocompatible profile towards both cancer and healthy cells, even after 48 h of incubation (viability > 86 %) – Figure 17. The good cytocompatibility of the Gel and IR/BPN@Gel is related with the excellent biocompatibility of chitosan-based hydrogels [86, 94, 95]. In fact, Lima-Sousa *et al.* also demonstrated the good cytocompatible profile of injectable *in situ* forming chitosan-agarose hydrogels [53]. Moreover, non-irradiated IR780 based nanomedicines are also generally cytocompatible [114-116]. Together, these results confirm the good cytocompatibility of the IR/BPN@Gel.

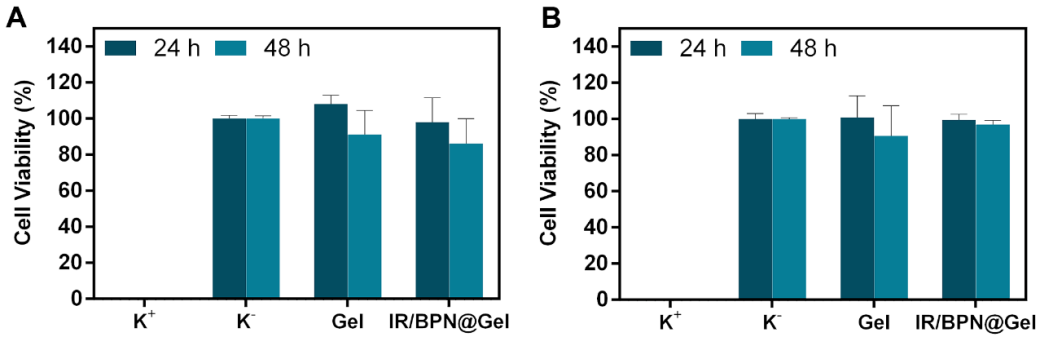

Figure 17 – Cell viability of MCF-7 (A) and NHDF (B) after incubation with Gel or IR/BPN@Gel for 24 and 48 h. Data represents mean ± S.D., n = 5. K^- represents the negative control and K^+ represents the positive control.

3.4. *In vitro* evaluation of the PTT mediated by IR/BPN@Gel and Chemo-PTT mediated by IR/BPN+DOX/TPN@Gel

Then, the therapeutic effect mediated by IR/BPN@Gel and IR/BPN+DOX/TPN@Gel towards MCF-7 cells was investigated. For such, cells were incubated with the hydrogel formulations and then were exposed to NIR light (808 nm, 1.7 W cm^{-2}, 10 min) – Figure 18A.

MCF-7 cells incubated with IR/BPN@Gel and exposed to NIR light experienced a reduction in their viability to about 35 % (Figure 18B). Such effect is related with the ability of the IR/BPN incorporated on this hydrogel to produce a photoinduced heat that can damage the cancer cells (Figure 13). As expected, cells solely incubated with IR/BPN@Gel or solely exposed to NIR light did not suffer any meaningful variation in their viability (Figure 18B). These results are justified by the good cytocompatible profile displayed by IR/BPN@Gel (Figure 17A) and by negligible off-targeting heating of water exposed to NIR light, respectively (Figure 13).

Xie *et al.* developed an agarose-based hydrogel incorporating black phosphorus nanosheets that, when irradiated with NIR light (1 mg of black phosphorus nanosheets; 808 nm, 0.925 W cm^{-2}, 10 min), induced a reduction in cancer cells' viability to 39 % [117]. Herein, the IR/BPN@Gel induced a similar reduction in the viability of cancer cells at an extremely lower dose of the photothermal nanoagent (3.73 μg mL^{-1} of IR780 equivalents) but at a higher laser intensity. These results attest the potential of IR/BPN@Gel for cancer PTT.

On the other hand, MCF-7 cells incubated with IR/BPN+DOX/TPN@Gel (3.29/0.71 μg mL^{-1} of IR780/DOX equivalents) remained with a viability of 85 %. However, when the cells were exposed to IR/BPN+DOX/TPN@Gel plus NIR light, their viability suffered a stark decrease to 9 % (Figure 18B). In this way, the improved therapeutic outcome attained by conjugating IR/BPN+DOX/TPN@Gel with NIR light is explained by the combined action of the chemo-photothermal effect and by the NIR-light enhanced DOX release (Figure 14).

Jiang *et al.* prepared a poly(ethylene glycol)-based hydrogel incorporating palladium nanosheets and DOX that, after NIR-light exposure (60/1 μg mL^{-1} of palladium/DOX; 808 nm, 0.6 W cm^{-2}, 10 min), reduced the cancer cells' viability to about 20 % [79]. In another study, injectable *in situ* forming chitosan-agarose hydrogels incorporating reduced graphene oxide (10 μg mL^{-1}) and a DOX:Ibuprofen combination (90.4 μM of the 1:5 DOX:Ibuprofen combination) could decrease MCF-7 cells' viability to 34 % after irradiation with NIR light (808 nm, 1.7 W cm^{-2}, 10 min) [53]. Herein, the Chemo-PTT mediated by IR/BPN+DOX/TPN@Gel diminished the MCF-7 cells' viability to only 9 %, using a very low dose of therapeutic nanoagents (3.29/0.71 μg mL^{-1} of IR780/DOX equivalents) and at a similar/higher radiation intensity (1.7 W cm^{-2}). In this way, the IR/BPN+DOX/TPN@Gel revealed to be a promising injectable *in situ* forming hydrogel that has potential for being applied in the Chemo-PTT of breast cancer.

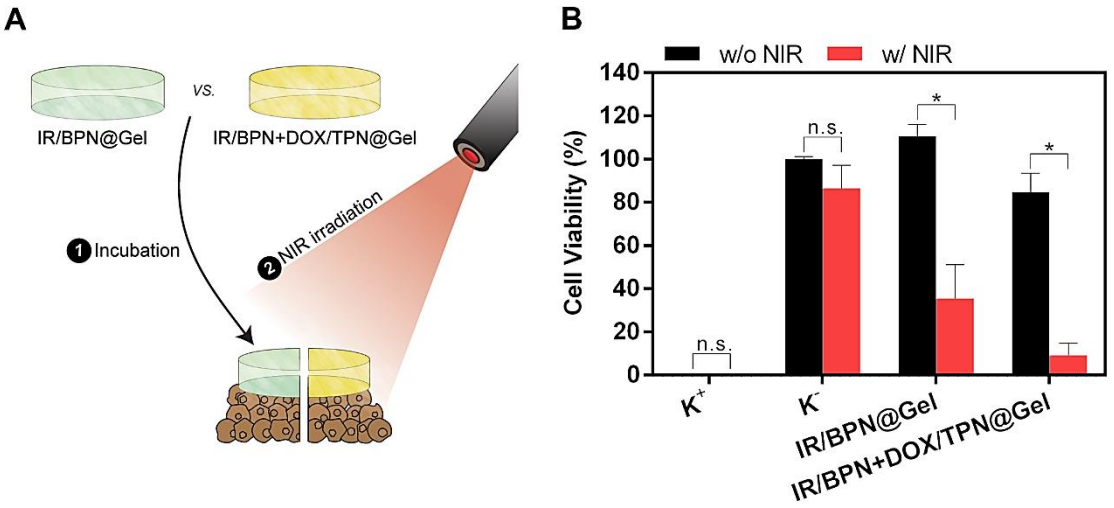

Figure 18 – Characterization of the phototherapeutic effect mediated by IR/BPN@Gel and IR/BPN+DOX/TPN@Gel. Schematic representation of the PTT and Chemo-PTT mediated by IR/BPN@Gel and IR/BPN+DOX/TPN@Gel, respectively (A). Phototherapeutic effect of IR/BPN@Gel (3.73 μg mL^{-1} of IR780 equivalents) and IR/BPN+DOX/TPN@Gel (3.29/0.71 μg mL^{-1} of IR780/DOX equivalents) towards MCF-7 cells without (w/o NIR) or with (w/ NIR) NIR laser irradiation (808 nm, 1.7 W cm^{-2}, 10 min). Data represents mean ± S.D., n = 5. (* $p < 0.0001$), n.s. = non-significant (B).

Chapter 4

Conclusion and Future Perspectives

4. Conclusion and Future Perspectives

Breast cancer still remains as one of the deadliest diseases affecting women. This situation can be explained by the low efficacy and by the undesirable side effects associated with the conventional therapies (*e.g*. chemotherapy or radiotherapy) used in the clinic.

To address these limitations, researchers have been exploring the therapeutic potential of nanomaterials' mediated Chemo-PTT. This therapeutic modality aims to attain synergistic effects by combining the action of the NIR light-induced heating and chemotherapeutic agents' delivery mediated by nanomaterials. Furthermore, the photoinduced heating can also prompt the release of the drugs, further improving the therapeutic outcome. Nonetheless, the median of the nanoparticles' dose accumulated at the tumor site after intravenous injection is usually below 1 %. To overcome this bottleneck, it is of utmost importance to develop innovative strategies that are able to perform the deliver nanomaterials directly into the tumor site.

In this MSc Dissertation, an injectable *in situ* forming ionotropically crosslinked chitosan-based hydrogel was developed. Then, IR/BPN and DOX/TPN were incorporated in the hydrogel in order to explore its applicability in cancer Chemo-PTT. The results obtained revealed that the IR/BPN@Gel and IR/BPN+DOX/TPN@Gel present suitable physicochemical properties. Upon NIR light exposure, the IR/BPN@Gel and IR/BPN+DOX/TPN@Gel produced a temperature increase of 9.2 °C and 9.0 °C, respectively, confirming their photothermal capacity. As importantly, the NIR-light exposure also increased the release of DOX from the hydrogel by 1.7 times, after 48 h. In the *in vitro* studies, the IR/BPN@Gel displayed cytocompatibility towards breast cancer and normal cells. Moreover, the combination of IR/BPN@Gel with NIR light (photothermal therapy) led to a reduction in the viability of breast cancer cells to 35 %. On the other hand, the non-irradiated IR/BPN+DOX/TPN@Gel (chemotherapy) only diminished the viability of cancer cells to 85 %. In stark contrast, the Chemo-PTT mediated by IR/BPN+DOX/TPN@Gel reduced the viability of the cancer cells to about 9 %. Overall, the IR/BPN+DOX/TPN@Gel is an injectable *in situ* forming hydrogel with great potential for the Chemo-PTT of breast cancer cells.

In the future, it will be interesting to explore the chemo-photothermal effect of IR/BPN+DOX/TPN@Gel in spheroids. These 3D *in vitro* models have the ability to mimic several features presented by solid tumors, such as their 3D architecture and biochemical/physical resistance patterns [118, 119]. Furthermore, *in vivo* studies will be crucial to determine the Chemo-PTT potential of IR/BPN+DOX/TPN@Gel as well as the hydrogel's biocompatibility and biodegradability. On the other hand, these hydrogels may incorporate other agents, enabling their use in more advanced therapeutic modalities (*e.g*. immunotherapy conjugated with Chemo-PTT) or in theragnostic applications (*e.g*. magnetic resonance imaging combined with Chemo-PTT).

Chapter 5

Bibliographic References

5. Bibliographic References

1. Siegel, R.L., K.D. Miller, and A. Jemal, *Cancer statistics, 2020*. CA: A Cancer Journal for Clinicians, 2020. **70**(1): p. 7-30.
2. *Cancer in Portugal*. Available from: https://observador.pt/2019/05/14/cancro-os-numeros-que-ja-sao-uma-realidade/ (acessed in 29/09/2020).
3. Carlberg, C. and F. Molnár, *Cancer Epigenetics*, in *Human Epigenetics: How Science Works*. 2019, Springer. p. 89-99.
4. Hanahan, D. and R.A. Weinberg, *Hallmarks of Cancer: The Next Generation*. Cell, 2011. **144**(5): p. 646-674.
5. Witsch, E., M. Sela, and Y. Yarden, *Roles for Growth Factors in Cancer Progression*. Physiology, 2010. **25**(2): p. 85-101.
6. Letai, A., *Apoptosis and Cancer*. Annual Review of Cancer Biology, 2017. **1**: p. 275-294.
7. Yip, K. and J. Reed, *Bcl-2 family proteins and cancer*. Oncogene, 2008. **27**(50): p. 6398-6406.
8. Mokbel, K. and K. Mokbel, *Apoptosis and Carcinogenesis: An Update*. Journal of Tumor, 2018. **6**(1): p. 520-525.
9. Perera, O.N., et al., *Telomerase promotes formation of a telomere protective complex in cancer cells*. Science Advances, 2019. **5**(10): p. 1-14.
10. *Studying Hallmarks of Cancer*. Available from: https://www.abcam.com/cancer/studying-hallmarks-of-cancer (acessed in 01/09/2020).
11. Lugano, R., M. Ramachandran, and A. Dimberg, *Tumor angiogenesis: causes, consequences, challenges and opportunities*. Cellular and Molecular Life Sciences, 2020. **77**(9): p. 1745-1770.
12. Riggi, N., M. Aguet, and I. Stamenkovic, *Cancer Metastasis: A Reappraisal of Its Underlying Mechanisms and Their Relevance to Treatment*. Annual Review of Pathology: Mechanisms of Disease, 2018. **13**: p. 117-140.
13. Welch, D.R. and D.R. Hurst, *Defining the Hallmarks of Metastasis*. Cancer Research, 2019. **79**(12): p. 3011-3027.
14. DeBerardinis, R.J. and N.S. Chandel, *Fundamentals of cancer metabolism*. Science Advances, 2016. **2**(5): p. 1-18.
15. Biswas, S.K., *Metabolic Reprogramming of Immune Cells in Cancer Progression*. Immunity, 2015. **43**(3): p. 435-449.
16. Polyak, K., *Heterogeneity in breast cancer*. The Journal of Clinical Investigation, 2011. **121**(10): p. 3786-3788.
17. DeSantis, C.E., et al., *Breast cancer statistics, 2019*. CA: A Cancer Journal for Clinicians, 2019. **69**(6): p. 438-451.
18. *Breast Cancer in Portugal*. Available from: https://www.ligacontracancro.pt/cancro-da-mama/ (acessed in 17/03/2020).

19. McPherson, K., C. Steel, and J. Dixon, *Breast cancer—epidemiology, risk factors, and genetics*. BMJ, 2000. **321**(7261): p. 624-628.
20. Momenimovahed, Z. and H. Salehiniya, *Epidemiological characteristics of and risk factors for breast cancer in the world*. Breast Cancer: Targets and Therapy, 2019. **11**: p. 151-164.
21. Sims, A.H., et al., *Origins of breast cancer subtypes and therapeutic implications*. Nature Clinical Practice Oncology, 2007. **4**(9): p. 516-525.
22. Hinohara, K. and K. Polyak, *Intratumoral Heterogeneity: More Than Just Mutations*. Trends in Cell Biology, 2019. **29**(7): p. 569-579.
23. Polyak, K., *Breast cancer: origins and evolution*. The Journal of Clinical Investigation, 2007. **117**(11): p. 3155-3163.
24. Zhou, J., et al., *Stem Cells and Cellular Origins of Breast Cancer: Updates in Rationale, Controversies and Therapeutic Implications*. Frontiers in Oncology, 2019. **9**(820): p. 1-12.
25. Kalinowski, L., et al., *Breast Cancer Heterogeneity in Primary and Metastatic Disease*, in *Breast Cancer Metastasis and Drug Resistance*. 2019, Springer. p. 75-104.
26. Di Wu, M.S., H.-Y. Xue, and H.-L. Wong, *Nanomedicine applications in the treatment of breast cancer: current state of the art*. International Journal of Nanomedicine, 2017. **12**: p. 5879-5892.
27. Tao, Z., et al., *Breast Cancer: Epidemiology and Etiology*. Cell Biochemistry and Biophysics, 2015. **72**(2): p. 333-338.
28. Chang, L., et al., *Breast cancer treatment and its effects on aging*. Journal of Geriatric Oncology, 2019. **10**(2): p. 346-355.
29. Bukowski, K., M. Kciuk, and R. Kontek, *Mechanisms of Multidrug Resistance in Cancer Chemotherapy*. International Journal of Molecular Sciences, 2020. **21**(9): p. 1-24.
30. Cao, J., et al., *Recent progress in synergistic chemotherapy and phototherapy by targeted drug delivery systems for cancer treatment*. Artificial Cells, Nanomedicine, and Biotechnology, 2018. **46**(S1): p. S817-S830.
31. Bertolini, F., V.P. Sukhatme, and G. Bouche, *Drug repurposing in oncology—patient and health systems opportunities*. Nature Reviews Clinical Oncology, 2015. **12**(12): p. 732-742.
32. Al-Dimassi, S., T. Abou-Antoun, and M. El-Sibai, *Cancer cell resistance mechanisms: a mini review*. Clinical and Translational Oncology, 2014. **16**(6): p. 511-516.
33. Al-Lazikani, B., U. Banerji, and P. Workman, *Combinatorial drug therapy for cancer in the post-genomic era*. Nature Biotechnology, 2012. **30**(7): p. 679-692.
34. Gaspar, V.M., et al., *Gas-generating TPGS-PLGA microspheres loaded with nanoparticles (NIMPS) for co-delivery of minicircle DNA and anti-tumoral drugs*. Colloids and Surfaces B: Biointerfaces, 2015. **134**: p. 287-294.
35. Dai, W., et al., *Combination antitumor therapy with targeted dual-nanomedicines*. Advanced Drug Delivery Reviews, 2017. **115**: p. 23-45.

36. Rahoui, N., et al., *Spatio-temporal control strategy of drug delivery systems based nano structures*. Journal of Controlled Release, 2017. **255**: p. 176-201.
37. Rodrigues, C.F., et al., *Inorganic-based drug delivery systems for cancer therapy*, in *Advances and Avenues in the Development of Novel Carriers for Bioactives and Biological Agents*. 2020, Elsevier. p. 283-316.
38. Kumar, C.S. and F. Mohammad, *Magnetic nanomaterials for hyperthermia-based therapy and controlled drug delivery*. Advanced Drug Delivery Reviews, 2011. **63**(9): p. 789-808.
39. Sharma, S., et al., *Nanoparticles-based magnetic and photo induced hyperthermia for cancer treatment*. Nano Today, 2019. **29**: p. 1-27.
40. de Melo-Diogo, D., et al., *Strategies to Improve Cancer Photothermal Therapy Mediated by Nanomaterials*. Advanced Healthcare Materials, 2017. **6**(10): p. 1-20.
41. Maghari, S. and A. Ghassempour, *Evaluation of protein corona formation and anticancer efficiency of curcumin-loaded zwitterionic silica nanoparticles*. Nanomedicine Journal, 2020. **7**(2): p. 149-157.
42. Cui, J., et al., *Ligand-Functionalized Poly(ethylene glycol) Particles for Tumor Targeting and Intracellular Uptake*. Biomacromolecules, 2019. **20**(9): p. 3592-3600.
43. Alves, C.G., et al., *Hyaluronic acid functionalized nanoparticles loaded with IR780 and DOX for cancer chemo-photothermal therapy*. European Journal of Pharmaceutics and Biopharmaceutics, 2019. **137**: p. 86-94.
44. Arabi, L., et al., *Targeting CD44 expressing cancer cells with anti-CD44 monoclonal antibody improves cellular uptake and antitumor efficacy of liposomal doxorubicin*. Journal of Controlled Release, 2015. **220**(A): p. 275-286.
45. Zheng, G., et al., *Improving breast cancer therapy using doxorubicin loaded solid lipid nanoparticles: Synthesis of a novel arginine-glycine-aspartic tripeptide conjugated, pH sensitive lipid and evaluation of the nanomedicine in vitro and in vivo*. Biomedicine & Pharmacotherapy, 2019. **116**: p. 1-10.
46. Jiang, Y., et al., *Co-Delivery of Paclitaxel and Doxorubicin by pH-Responsive Prodrug Micelles for Cancer Therapy*. International Journal of Nanomedicine, 2020. **15**: p. 3319-3331.
47. Qu, M.-H., et al., *Liposome-based co-delivery of siRNA and docetaxel for the synergistic treatment of lung cancer*. International Journal of Pharmaceutics, 2014. **474**(1-2): p. 112-122.
48. Tiwari, H., et al., *Functionalized graphene oxide as a nanocarrier for dual drug delivery applications: The synergistic effect of quercetin and gefitinib against ovarian cancer cells*. Colloids and Surfaces B: Biointerfaces, 2019. **178**: p. 452-459.
49. Morton, S.W., et al., *A Nanoparticle-Based Combination Chemotherapy Delivery System for Enhanced Tumor Killing by Dynamic Rewiring of Signaling Pathways*. Science Signaling, 2014. **7**(325): p. 1-11.

50. Kumar, B., et al., *Redox responsive xylan-SS-curcumin prodrug nanoparticles for dual drug delivery in cancer therapy*. Materials Science and Engineering: C, 2020. **107**: p. 1-11.
51. Ghaffari, M., et al., *Co-delivery of curcumin and Bcl-2 siRNA by PAMAM dendrimers for enhancement of the therapeutic efficacy in HeLa cancer cells*. Colloids and Surfaces B: Biointerfaces, 2020. **188**: p. 1-11.
52. Hao, Y., et al., *Near-infrared responsive 5-fluorouracil and indocyanine green loaded MPEG-PCL nanoparticle integrated with dissolvable microneedle for skin cancer therapy*. Bioactive Materials, 2020. **5**(3): p. 542-552.
53. Lima-Sousa, R., et al., *Injectable in situ forming thermo-responsive graphene based hydrogels for cancer chemo-photothermal therapy and NIR light-enhanced antibacterial applications*. Materials Science and Engineering: C, 2020. **117**: p. 1-8.
54. Yan, F., et al., *NIR-Laser-Controlled Drug Release from DOX/IR-780-Loaded Temperature-Sensitive-Liposomes for Chemo-Photothermal Synergistic Tumor Therapy*. Theranostics, 2016. **6**(13): p. 2337-2351.
55. de Melo-Diogo, D., et al., *POxylated graphene oxide nanomaterials for combination chemo-phototherapy of breast cancer cells*. European Journal of Pharmaceutics and Biopharmaceutics, 2018. **131**: p. 162-169.
56. Zheng, M., et al., *Single-Step Assembly of DOX/ICG Loaded Lipid–Polymer Nanoparticles for Highly Effective Chemo-photothermal Combination Therapy*. ACS Nano, 2013. **7**(3): p. 2056-2067.
57. Pan, Q., et al., *Tumor-Targeting Polycaprolactone Nanoparticles with Codelivery of Paclitaxel and IR780 for Combinational Therapy of Drug-Resistant Ovarian Cancer*. ACS Biomaterials Science & Engineering, 2020. **6**(4): p. 2175-2185.
58. Khafaji, M., et al., *Inorganic nanomaterials for chemo/photothermal therapy: a promising horizon on effective cancer treatment*. Biophysical Reviews, 2019. **11**: p. 335-352.
59. Weng, Y., et al., *Defective Porous Carbon Polyhedra Decorated with Copper Nanoparticles for Enhanced NIR-Driven Photothermal Cancer Therapy*. Small, 2020. **16**(1): p. 1-10.
60. Lima-Sousa, R., et al., *Hyaluronic acid functionalized green reduced graphene oxide for targeted cancer photothermal therapy*. Carbohydrate Polymers, 2018. **200**: p. 93-99.
61. Park, S., et al., *Reversibly pH-responsive gold nanoparticles and their applications for photothermal cancer therapy*. Scientific Reports, 2019. **9**(1): p. 1-9.
62. Yoon, H.-J., et al., *Liposomal Indocyanine Green for Enhanced Photothermal Therapy*. ACS Applied Materials & Interfaces, 2017. **9**(7): p. 5683-5691.
63. Lee, S., et al., *Near-Infrared Heptamethine Cyanine Based Iron Oxide Nanoparticles for Tumor Targeted Multimodal Imaging and Photothermal Therapy*. Scientific Reports, 2017. **7**(1): p. 1-14.

64. Liu, M., et al., *An injectable nanocomposite hydrogel co-constructed with gold nanorods and paclitaxel-loaded nanoparticles for local chemo-photothermal synergetic cancer therapy*. Journal of Materials Chemistry B, 2019. **7**(16): p. 2667-2677.
65. Mirrahimi, M., et al., *A thermo-responsive alginate nanogel platform co-loaded with gold nanoparticles and cisplatin for combined cancer chemo-photothermal therapy*. Pharmacological Research, 2019. **143**: p. 178-185.
66. Mirrahimi, M., et al., *Triple combination of heat, drug and radiation using alginate hydrogel co-loaded with gold nanoparticles and cisplatin for locally synergistic cancer therapy*. International Journal of Biological Macromolecules, 2020. **158**: p. 617-626.
67. Chen, Y., et al., *IR-780 Loaded Phospholipid Mimicking Homopolymeric Micelles for Near-IR Imaging and Photothermal Therapy of Pancreatic Cancer*. ACS Applied Materials & Interfaces, 2016. **8**(11): p. 6852-6858.
68. Jiang, C., et al., *Hydrophobic IR780 encapsulated in biodegradable human serum albumin nanoparticles for photothermal and photodynamic therapy*. Acta Biomaterialia, 2015. **14**: p. 61-69.
69. Zhu, H., et al., *Recent progress in the development of near-infrared organic photothermal and photodynamic nanotherapeutics*. Biomaterials Science, 2018. **6**(4): p. 746-765.
70. Li, Z., et al., *Recent Advances in Nanomaterials-Based Chemo-Photothermal Combination Therapy for Improving Cancer Treatment*. Frontiers in Bioengineering and Biotechnology, 2019. **7**(293): p. 1-19.
71. Alves, C.G., et al., *IR780 based nanomaterials for cancer imaging and photothermal, photodynamic and combinatorial therapies*. International Journal of Pharmaceutics, 2018. **542**(1-2): p. 164-175.
72. Cheng, Y., et al., *Perfluorocarbon nanoparticles enhance reactive oxygen levels and tumour growth inhibition in photodynamic therapy*. Nature Communications, 2015. **6**(8785): p. 1-8.
73. Wilhelm, S., et al., *Analysis of nanoparticle delivery to tumours*. Nature Reviews Materials, 2016. **1**(5): p. 1-12.
74. Liu, H. and S.S. Venkatraman, *Cosolvent Effects on the Drug Release and Depot Swelling in Injectable In situ Depot-Forming Systems*. Journal of Pharmaceutical Sciences, 2012. **101**(5): p. 1783-1793.
75. Talebian, S., et al., *Biopolymers for Antitumor Implantable Drug Delivery Systems: Recent Advances and Future Outlook*. Advanced Materials, 2018. **30**(31): p. 1-31.
76. Fakhari, A. and J.A. Subramony, *Engineered in-situ depot-forming hydrogels for intratumoral drug delivery*. Journal of Controlled Release, 2015. **220**(A): p. 465-475.
77. Jonas, O., et al., *An implantable microdevice to perform high-throughput in vivo drug sensitivity testing in tumors*. Science Translational Medicine, 2015. **7**(284): p. 1-12.
78. Geng, S., et al., *Injectable in Situ Forming Hydrogels of Thermosensitive Polypyrrole Nanoplatforms for Precisely Synergistic Photothermo-Chemotherapy*. ACS Applied Materials & Interfaces, 2020. **12**(7): p. 7995-8005.

79. Jiang, Y.-W., et al., *Palladium nanosheet-knotted injectable hydrogels formed via palladium–sulfur bonding for synergistic chemo-photothermal therapy*. Nanoscale, 2020. **12**(1): p. 210-219.
80. Wang, L., et al., *UV-crosslinkable and thermo-responsive chitosan hybrid hydrogel for NIR-triggered localized on-demand drug delivery*. Carbohydrate Polymers, 2017. **174**: p. 904-914.
81. Lee, J.H., *Injectable hydrogels delivering therapeutic agents for disease treatment and tissue engineering*. Biomaterials Research, 2018. **22**(27): p. 1-14.
82. Mathew, A.P., et al., *Injectable hydrogels for delivering biotherapeutic molecules*. International Journal of Biological Macromolecules, 2018. **110**: p. 17-29.
83. Chhibber, T., et al., *Hydrogels in Tissue Engineering*, in *Intelligent Hydrogels in Diagnostics and Therapeutics*. 2020, CRC Press. p. 105-122.
84. Nguyen, Q.V., J.H. Park, and D.S. Lee, *Injectable polymeric hydrogels for the delivery of therapeutic agents: A review*. European Polymer Journal, 2015. **72**: p. 602-619.
85. Huang, P., et al., *Bridging the Gap between Macroscale Drug Delivery Systems and Nanomedicines: A Nanoparticle-Assembled Thermosensitive Hydrogel for Peritumoral Chemotherapy*. ACS Applied Materials & Interfaces, 2016. **8**(43): p. 29323-29333.
86. Peers, S., A. Montembault, and C. Ladavière, *Chitosan hydrogels for sustained drug delivery*. Journal of Controlled Release, 2020. **326**: p. 150-163.
87. Norouzi, M., B. Nazari, and D.W. Miller, *Injectable hydrogel-based drug delivery systems for local cancer therapy*. Drug Discovery Today, 2016. **21**(11): p. 1835-1849.
88. Kearney, C.J. and D.J. Mooney, *Macroscale delivery systems for molecular and cellular payloads*. Nature Materials, 2013. **12**(11): p. 1004-1017.
89. Zheng, Y., et al., *Preparation of injectable temperature-sensitive chitosan-based hydrogel for combined hyperthermia and chemotherapy of colon cancer*. Carbohydrate Polymers, 2019. **222**: p. 1-11.
90. Zhao, J., et al., *Fe^{3+}-Induced Synchronous Formation of Composite Hydrogels for Effective Synergistic Tumor Therapy in NIR-I/II Biowindows*. ACS Applied Materials & Interfaces, 2018. **10**(49): p. 41947-41955.
91. Berger, J., et al., *Structure and interactions in chitosan hydrogels formed by complexation or aggregation for biomedical applications*. European Journal of Pharmaceutics and Biopharmaceutics, 2004. **57**(1): p. 35-52.
92. Abasalizadeh, F., et al., *Alginate-based hydrogels as drug delivery vehicles in cancer treatment and their applications in wound dressing and 3D bioprinting*. Journal of Biological Engineering, 2020. **14**(8): p. 1-22.
93. Wang, X., et al., *Defective Black Nano-Titania Thermogels for Cutaneous Tumor-Induced Therapy and Healing*. Nano Letters, 2019. **19**(3): p. 2138-2147.
94. Hamedi, H., et al., *Chitosan based hydrogels and their applications for drug delivery in wound dressings: A review*. Carbohydrate Polymers, 2018. **199**: p. 445-460.
95. Miguel, S.P., et al., *Thermoresponsive chitosan–agarose hydrogel for skin regeneration*. Carbohydrate Polymers, 2014. **111**: p. 366-373.

96. Galisteo-González, F. and J. Molina-Bolívar, *Systematic study on the preparation of BSA nanoparticles*. Colloids and Surfaces B: Biointerfaces, 2014. **123**: p. 286-292.
97. Liu, T., et al., *Mechanisms of TPGS and its derivatives inhibiting P-glycoprotein efflux pump and application for reversing multidrug resistance in hepatocellular carcinoma*. Polymer Chemistry, 2018. **9**(14): p. 1827-1839.
98. Yang, C., et al., *Recent Advances in the Application of Vitamin E TPGS for Drug Delivery*. Theranostics, 2018. **8**(2): p. 464-485.
99. Alves, C.G., et al., *IR780 loaded sulfobetaine methacrylate-functionalized albumin nanoparticles aimed for enhanced breast cancer phototherapy*. International Journal of Pharmaceutics, 2020. **582**: p. 1-9.
100. Pais-Silva, C., D. de Melo-Diogo, and I.J. Correia, *IR780-loaded TPGS-TOS micelles for breast cancer photodynamic therapy*. European Journal of Pharmaceutics and Biopharmaceutics, 2017. **113**: p. 108-117.
101. Cabral, C.S., et al., *Green reduced graphene oxide functionalized 3D printed scaffolds for bone tissue regeneration*. Carbon, 2019. **146**: p. 513-523.
102. de Melo-Diogo, D., et al., *D-α-tocopheryl polyethylene glycol 1000 succinate functionalized nanographene oxide for cancer therapy*. Nanomedicine, 2017. **12**(5): p. 443-456.
103. Guo, Y., et al., *The applications of Vitamin E TPGS in drug delivery*. European Journal of Pharmaceutical Sciences, 2013. **49**(2): p. 175-186.
104. Wang, A.Z., R. Langer, and O.C. Farokhzad, *Nanoparticle Delivery of Cancer Drugs*. Annual Review of Medicine, 2012. **63**: p. 185-198.
105. Stern, T., et al., *Rigidity of polymer micelles affects interactions with tumor cells*. Journal of Controlled Release, 2017. **257**: p. 40-50.
106. Durymanov, M., et al., *Role of Endocytosis in Nanoparticle Penetration of 3D Pancreatic Cancer Spheroids*. Molecular Pharmaceutics, 2019. **16**(3): p. 1074-1082.
107. Ferrado, J.B., et al., *Formation and characterization of self-assembled bovine serum albumin nanoparticles as chrysin delivery systems*. Colloids and Surfaces B: Biointerfaces, 2019. **173**: p. 43-51.
108. Liu, B.-Y., et al., *Multi-drug loaded vitamin E-TPGS nanoparticles for synergistic drug delivery to overcome drug resistance in tumor treatment*. Science Bulletin, 2016. **61**(7): p. 552-560.
109. Arora, D., et al., *Preparation, characterization and cytotoxic evaluation of bovine serum albumin nanoparticles encapsulating 5-methylmellein: A secondary metabolite isolated from Xylaria psidii*. Bioorganic & Medicinal Chemistry Letters, 2017. **27**(23): p. 5126-5130.
110. Pan, J. and S.-S. Feng, *Targeted delivery of paclitaxel using folate-decorated poly(lactide)–vitamin E TPGS nanoparticles*. Biomaterials, 2008. **29**(17): p. 2663-2672.
111. Singh, Y.P., N. Bhardwaj, and B.B. Mandal, *Potential of Agarose/Silk Fibroin Blended Hydrogel for in Vitro Cartilage Tissue Engineering*. ACS Applied Materials & Interfaces, 2016. **8**(33): p. 21236-21249.

112. Wang, H., et al., *Biocompatible Iodine–Starch–Alginate Hydrogel for Tumor Photothermal Therapy*. ACS Biomaterials Science & Engineering, 2019. **5**(7): p. 3654-3662.
113. Gai, S., et al., *Recent advances in functional nanomaterials for light–triggered cancer therapy*. Nano Today, 2018. **19**: p. 146-187.
114. Kuang, Y., et al., *Hydrophobic IR-780 Dye Encapsulated in cRGD-Conjugated Solid Lipid Nanoparticles for NIR Imaging-Guided Photothermal Therapy*. ACS Applied Materials & Interfaces, 2017. **9**(14): p. 12217-12226.
115. Song, J., et al., *IR780-loaded folate-targeted nanoparticles for near-infrared fluorescence image-guided surgery and photothermal therapy in ovarian cancer*. International Journal of Nanomedicine, 2019. **14**: p. 2757-2772.
116. Lin, S.-Y., et al., *Multifunctional PEGylated Albumin/IR780/Iron Oxide Nanocomplexes for Cancer Photothermal Therapy and MR Imaging*. Nanotheranostics, 2018. **2**(2): p. 106-116.
117. Xie, J., et al., *Emetine-Loaded Black Phosphorus Hydrogel Sensitizes Tumor to Photothermal Therapy through Inhibition of Stress Granule Formation*. Advanced Functional Materials, 2020. **30**(43): p. 1-8.
118. Nunes, A.S., et al., *3D tumor spheroids as in vitro models to mimic in vivo human solid tumors resistance to therapeutic drugs*. Biotechnology and Bioengineering, 2019. **116**(1): p. 206-226.
119. Barros, A.S., et al., *Comparative study of the therapeutic effect of Doxorubicin and Resveratrol combination on 2D and 3D (spheroids) cell culture models*. International Journal of Pharmaceutics, 2018. **551**(1-2): p. 76-83.